Journal of Medicinal Chemistry

Drug Annotation

pubs.acs.org/jmc

Discovery of a Potent and Selective EGFR Inhibitor (AZD9291) of Both Sensitizing and T790M Resistance Mutations That Spares the Wild Type Form of the Receptor

M. Raymond V. Finlay,*[,†] Mark Anderton,[‡] Susan Ashton,[†] Peter Ballard,[†] Paul A. Bethel,[†] Matthew R. Box,[†] Robert H. Bradbury,[†] Simon J. Brown,[†] Sam Butterworth,[†] Andrew Campbell,[†] Christopher Chorley,[†] Nicola Colclough,[‡] Darren A. E. Cross,[†] Gordon S. Currie,[†] Matthew Grist,[†] Lorraine Hassall,[†] George B. Hill,[†] Daniel James,[†] Michael James,[†] Paul Kemmitt,[†] Teresa Klinowska,[†] Gillian Lamont,[†] Scott G. Lamont,[†] Nathaniel Martin,[†] Heather L. McFarland,[§] Martine J. Mellor,[†] Jonathon P. Orme,[∥] David Perkins,[†] Paula Perkins,[†] Graham Richmond,[†] Peter Smith,[†] Richard A. Ward,[†] Michael J. Waring,[†] David Whittaker,[†] Stuart Wells,[†] and Gail L. Wrigley[†]

[†]Oncology Innovative Medicines, [‡]Drug Safety and Metabolism, [§]Global Medicines Development, and [∥]Discovery Sciences, AstraZeneca, Mereside, Alderley Park, Macclesfield, Cheshire SK10 4TG, U.K.

Supporting Information

ABSTRACT: Epidermal growth factor receptor (EGFR) inhibitors have been used clinically in the treatment of non-small-cell lung cancer (NSCLC) patients harboring sensitizing (or activating) mutations for a number of years. Despite encouraging clinical efficacy with these agents, in many patients resistance develops leading to disease progression. In most cases, this resistance is in the form of the T790M mutation. In addition, EGFR wild type receptor inhibition inherent with these agents can lead to dose limiting toxicities of rash and diarrhea. We describe herein the evolution of an early, mutant selective lead to the clinical candidate AZD9291, an irreversible inhibitor of both EGFR sensitizing (EGFRm+) and T790M resistance mutations with selectivity over the wild type form of the receptor. Following observations of significant tumor inhibition in preclinical models, the clinical candidate was administered clinically to patients with T790M positive EGFR-TKI resistant NSCLC and early efficacy has been observed, accompanied by an encouraging safety profile.

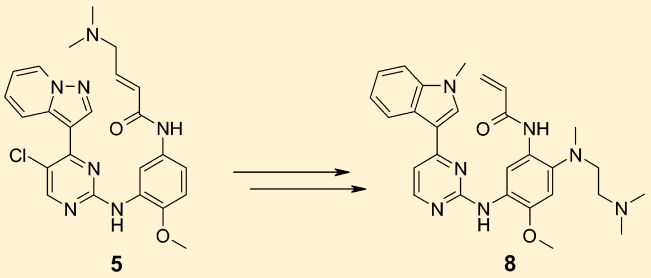

INTRODUCTION

The role of the epidermal growth factor receptor (EGFR) in non-small-cell lung cancer is well-known, and substantial therapeutic progress in the treatment of this disease has been made over the past 10 years through the exploitation of this insight.[1] Inhibition of the kinase domain of EGFR and resultant oncogenic cell signaling disruption by small molecule inhibitors such as gefitinib **1** and erlotinib **2** (Figure 1) have been shown to be particularly beneficial in those patients carrying the so-called "sensitizing mutations" such as L858R and the exon-19 deletion.[2,3] However, emergence of resistance to these targeted therapies continues to be a cause for concern, with the T790M mutation in particular being highlighted as a key therapeutic target.[4] The subsequent identification of irreversible EGFR inhibitors such as dacomitinib **3** and afatinib **4**[5] (Figure 1) that inhibit both mutants described above as well as the wild type receptor potentially offers therapeutic options for T790M positive patients. However, the high wild-type potency and accompanying toxicities associated with such activity may well limit their utility in this setting.

Recently, both ourselves[6] (compound **5**, Figure 2) and others[7,8] (*N*-[3-[5-chloro-2-[[2-methoxy-4-(4-methylpiperazin-1-yl)-phenyl]amino]pyrimidin-4-yl]oxyphenyl]prop-2-enamide (WZ-4002), **6**, Gatekeeper Pharmaceuticals Inc.; *N*-[3-[[2-[[4-(4-acetylpiperazin-1-yl)-2-methoxyphenyl]amino]-5-chloropyrimidin-4-yl]amino]phenyl]prop-2-enamide (CO-1686), **7**, Clovis Oncology) have described efforts to identify mutant selective inhibitors that target both the sensitizing mutations and the T790M resistance mutation while also sparing the wild type form of the receptor, inhibition of which can lead to dose limiting toxicities including skin rash and diarrhea. Herein, we describe some of our work that has led to the identification of the clinical candidate AZD9291 (**8**), a potent inhibitor of both sensitizing and double mutant (sensitizing and T790M resistance) forms of EGFR with selectivity over the wild type form (Figure 2).

RESULTS AND DISCUSSION

Previously, we had described our efforts in this area that culminated in the identification of **5**, a potent and selective EGFR inhibitor that had demonstrated in vivo efficacy in both activating

Received: June 27, 2014

   dx.doi.org/10.1021/jm500973a | *J. Med. Chem.* XXXX, XXX, XXX−XXX

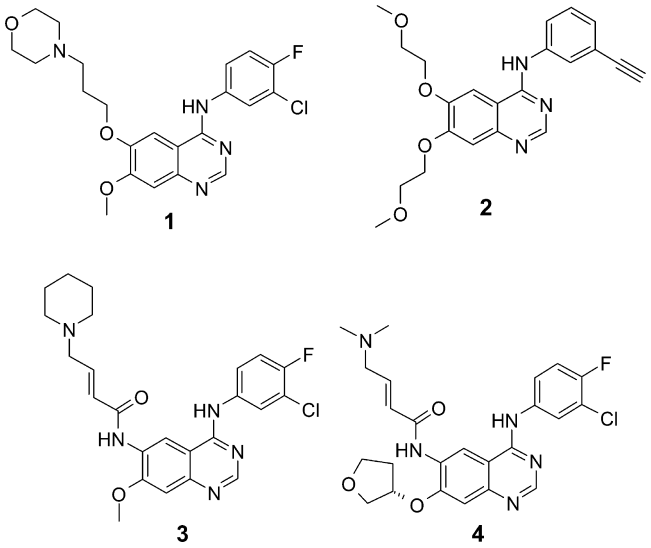

Figure 1. Structures of reversible and irreversible EGFR inhibitors.

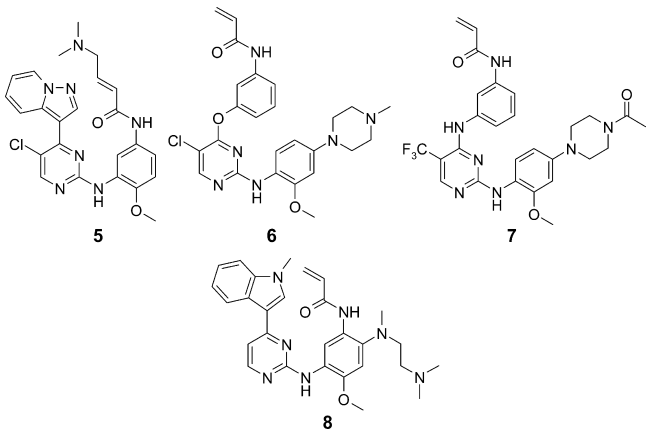

Figure 2. Mutant selective EGFR inhibitors.

and double mutant human xenograft disease models while also displaying minimal activity in a wild type setting.[6]

During the course of these studies, we had also identified **9** and **10** as potent and selective mutant EGFR inhibitors, where the pendent basic center, normally resident on the terminal position of the acrylamide, had been migrated to the aryl ring adjacent to the amide functionality. Our interest was piqued by this architectural modification for a number of reasons, not least of which was the improved potency offered by **10** for no apparent increase in lipophilicity. In our previous work,[6] we had encountered a log *D*/cell potency correlation whereby although cellular potency could be increased, it was generally accompanied by an increase in lipopilicity of the inhibitor compounds, and this tended to both increase their plasma protein binding and reduce their aqueous solubility. While compound **9** showed broadly similar double mutant potency to **5**, its reduced IGF1R activity and increased activating mutant activity again with no increase in lipophilicity were of great interest. Kinase selectivity for these inhibitors, as judged by profiling in a kinase selectivity screen (Dundee panel),[9a] appeared acceptable with only a small number of significant hits (Table 1). Compound **10** appeared to offer superior selectivity for the mutant forms of the receptor, although it should be noted that **9**, as mentioned above, did carry significantly less activity against the methionine gatekeeper bearing receptor tyrosine kinase IGF1R. A lipophilic group at the pyrimidine 5-position appears to offer a potentially favorable interaction with the methionine in both IGF1R and the double mutant ATP binding sites, and we reasoned that kinetic selectivity might be achievable because of irreversible binding to the double mutant, whereas the IGF1R interaction would be reversible. While IGF1R inhibitors have been employed in a clinical setting, their lack of selectivity with respect to inhibition of insulin receptor signaling has in some instances led to dose limiting toxicity and monitoring these effects can complicate study designs.[10] An additional driver for favoring **10** was that in contrast to **9**, it did offer modest exposure when dosed orally at 50 mg/kg in SCID mice. The aqueous solubility and hERG inhibition profile of **10** were also viewed as offering a good starting point, and we focused our initial efforts on further evolution of this lead.

Chemistry. A body of work focused on preparing amides of the distal piperazine nitrogen of **10** was first instigated. By use of chemistry similar to that described above (Scheme 1), fluoro intermediate **11**[6] was exposed to various piperazine amides bearing protected amino/hydroxyl groups. The nitro group was then reduced, and the resulting aniline was acylated with acryloyl chloride using the chemistry described previously. Protecting groups (either BOC or TBDMS) were then removed to afford the required compounds (Table 2).

A variety of alternative diamine reagents were available in house, and guided by a calculated lipophilicity threshold (log *D* of no more than 3 to try and maintain good physicochemical properties), we targeted the examples shown in Table 3. We employed our previously described chemistry to access these compounds, using late-stage fluoro intermediate **11** (Scheme 2).[6] Introduction of the amine side chain was achieved via S_NAr reaction; subsequent reduction of the nitro group and reaction with acryloyl chloride furnished the desired final compounds.

To access indole compounds **23**–**27** (Table 8), commercial pyrimidines with R2 = H, Me and Cl were used. Introduction of the indole was achieved by deprotonation with methylmagnesium bromide (Scheme 3) and subsequent S_NAR in adequate yield. Where R1 = Me, deprotonation of the indole NH and methylation with methyl iodide proceeded in good yield. Introduction of the aniline side chain and further elaboration into the desired compounds were achieved in a similar manner to the compounds detailed in Scheme 1.

In the case where R2 was cyano, this group was introduced at the penultimate step (Scheme 3). Although isolated in modest yield, this approach yielded sufficient material to deliver the desired compound.

As can be seen from Table 2, it became apparent that while initial compounds such as **12** and **13** offered reasonable potency profiles, all subsequent attempts to achieve further improvements provided less potent analogs, particularly against the activating mutant cell line. The enantiomeric pair of compounds **14** and **15** showed virtually identical cellular inhibition profiles, whereas in contrast, the enantiomeric pair of **13** and **19** did appear to favor the *S*-enantiomer. Removal of a methyl group from **12** to give **16** slightly reduced activity, and replacement of the NH_2 group of **13** with a hydroxyl to give **17** again reduced activity. The urea analogue **18** also led to modest levels of activity in cells. We concluded (particularly in the light of the emerging data for the basic side chain anlaogues; vide infra) that amides such as these did not offer the levels of potency to justify additional investigation, and these compounds were not pursued further.

dx.doi.org/10.1021/jm500973a | *J. Med. Chem.* XXXX, XXX, XXX−XXX

Table 1. Structures and Selected Properties of Lead Optimization Start Points

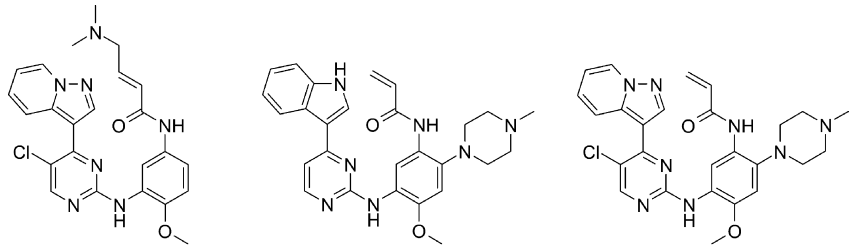

5 9 10

	5	9	10
DM cell IC_{50} (μM)[a]	0.091	0.063	0.019
AM cell IC_{50} (μM)[a]	0.388	0.015	0.14
WT cell IC_{50} (μM)[a]	>20	1.2	12
log $D_{7.4}$	3.6	3.4	3.6
LLE (DM cell)[b]	3.4	3.8	4.1
nude mouse po 50 mg/kg: C_{max} (μM), AUC (μM·h)	5.8, 67	0, 0	2.7, 13.4
mouse Heps Cl_{int} [(μL/min)/(10^6 cells)]	35	53	
solubility, pH 7.4 (μM)[c]	1	828	>973
hERG IC_{50} (μM)	4.2	9.1	7.1
IGF1R (enz) IC_{50} (μM)	0.004 (n = 1)	0.813 (n = 1)	0.002
kinase panel[d] hits (>90% inhibition at 1 μM)	CHK2 (90%) CAMKKβ (94%) IGF1R (98%) INSR (97%)	not tested	CAMKKβ (92%) IGF1R (97%)

[a]Inhibition of EGFR phosphorylation. All cell IC_{50} measurements reported are the geometric mean of at least two independent measurements unless otherwise indicated. The standard error of the mean (SEM) is not shown, as all three assays were found to be highly reproducible on repeat testing (pIC_{50} SEM typically <0.2; see Supporting Information for more detail). Because of the irreversible nature of inhibition of the compounds employed in this study, IC_{50} values are time dependent and are quoted as measured following an incubation period of 2 h. Double mutant (DM) cell line: H1975. Activating mutant exon 19 del (AM) cell line: PC9. Wild type (WT) cell line: LoVo. [b]Ligand lipophilicity efficiency (LLE) is calculated from DM cell pIC_{50} − log $D_{7.4}$. [c]Aqueous solubility measurement was performed under thermodynamic conditions using solid material. [d]MRC protein phosphorylation unit at the University of Dundee.[9a]

Scheme 1. General Synthesis of Piperazine Amides 12−19[a]

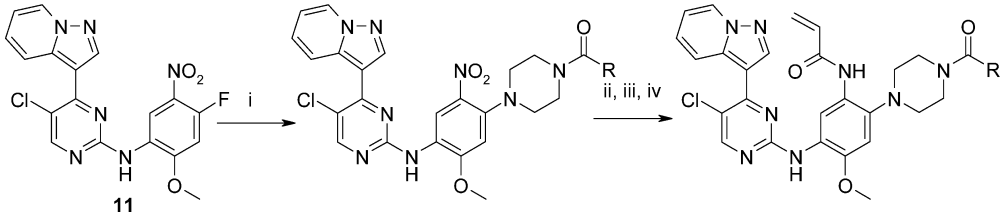

11

[a]Reagents and conditions: (i) piperazine amide, DIPEA, DMA, 140 °C (microwave); (ii) iron, NH_4Cl, EtOH, water, 100 °C; (iii) acryloyl chloride, DIPEA, DCM, 0 °C; (iv) functional group deprotection if required; TFA, DCM, rt; or TBAF, THF, rt.

A number of other carbon and oxygen linked basic side chains were also examined, but they offered little advantage in terms of potency, physical properties, or oral exposure when compared to the nitrogen linked systems described above. In contrast, the compounds where the piperazine group had been replaced with certain particular basic side chains produced a number of examples with exquisite cellular potency, in some cases being below 1 nM (Table 3). Of particular interest was the observation that the increase in potency observed did not come with increasing lipophilicity (as also noted for **9** and **10**), and in contrast to the previously described series with the pendent base on the acrylamide, the log D/cell potency correlation appeared to be weaker. Intrigued by these findings, we elected to further profile a variety of the most potent examples from this set. As can be seen from Table 3, the compounds showed excellent cellular potency against both mutants in phosphorylation and phenotypic antiproliferation assays with selectivity over wild type EGFR, log D values of around 3, modest aqueous solubility in pH 7.4 buffer, and acceptable free fractions in rat and human plasma. Table 3 also highlights the observation that the compounds again showed moderate affinity for the hERG channel and potent IGF1R activity in a similar fashion to **9** and **10**. Nevertheless, additional profiling in a broad kinase selectivity panel (Dundee panel,[9a] 1 μM) did show that the compounds possessed good overall kinase selectivity and had improved selectivity relative to **10** and **5**. We had previously[6] employed a glutathione (GSH) reaction assay to determine the relative reactivity of inhibitor compounds,[11−14] and the GSH reaction half-lives of these novel analogues fell within our earlier defined suitable "reactivity window". Interestingly, a small dependence of GSH half-life on the pK_a of the basic group is seen, suggestive of intramolecular base catalysis. The intrinsic clearance of the compounds was relatively high, but encouraged by the overall profile of the series, we elected to investigate the exposure of the compounds when

dx.doi.org/10.1021/jm500973a | J. Med. Chem. XXXX, XXX, XXX−XXX

Table 2. Structures and Selected Properties of Piperazine Amides 12−19

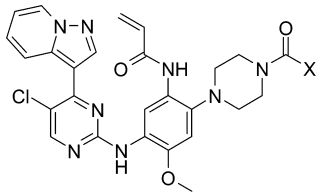

	12	13	14	15	16	17	18	19
X			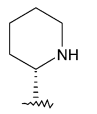	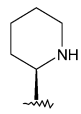			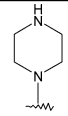	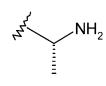
DM cell IC_{50} (nM)	16	19	31	57	66	75	135	177
AM cell IC_{50} (nM)	73	28	211	220	156	179	247	351
WT cell IC_{50} (nM)	10000	1600	6060	5600	7500	11000	10300	9000
$LogD_{7.4}$	2.6	-	2.2	2.2	1.8	-	2.0	2.1
LLE (DM cell)	5.2	-	5.3	5.0	5.4	-	4.9	4.7

dosed orally in the SCID mouse. Compounds were prioritized for in vivo work based on cell potency, free fraction, and aqueous solubility.

We selected **20** as our initial compound to be administered (the opposite enantiomer of **20** showed 2- to 3-fold less potency in cells), and as in our previous work,[6] we employed a 50 mg/kg once daily oral dose (Figure 3). The compound was well tolerated at this dose, and excellent exposure was observed. As can be seen from Table 4, the plasma levels achieved were substantial and well in excess of the concentrations needed to achieve free cover over the cellular IC_{50} values. As a consequence, for subsequent compounds in the series, we moved to 10 mg/kg as our initial dose. At this lower dose, multiples of free cover were still achieved for compounds **21** and **22** (although more modest in the latter, Table 4), and these inhibitors were selected for evaluation in a pharmacodynamic (PD) study.

A single dose of compounds **20**, **21**, and **22** were dosed orally in SCID mice at 10 mg/kg, and the percentage knockdown of EGFR phosphorylation in H1975 (double mutant) and PC9 (activating mutant) xenografts was measured compared to control (Tables 5 and 6 and Figures 4 and 5). All three compounds showed a profound effect on the PD biomarker. In the PC9 tumor cell line, **22** and **21** showed broadly similar effects with maximal inhibition (85% and 83% respectively) at the 6 h time point. Compound **20** showed slightly less biomarker modulation at this point, but in contrast to the other two compounds where p-EGFR levels began to return toward normal when measured at subsequent points, **20** continued to show sustained inhibition at the 24 h time point. In contrast, in the H1975 PD study, all three compounds showed sustained biomarker inhibition out to 24 h, although **21** now showed the most marked effect. By the 30 h time point, **22** inhibitory effects seemed to have been reduced whereas **21** still displayed a significant level of biomarker modulation. Given the clear evidence of in vivo effects on the target protein, the three compounds were selected for further evaluation in efficacy studies.

For this work, in vivo xenograft models representing the drug-resistant double mutant (H1975), sensitizing mutant (PC9), and wild type (A431) were selected. Compounds were dosed orally once a day for 7 days (Figure 6).

From examination of Figure 6, it can be seen that at 10 mg kg^{-1} day^{-1}, each of the compounds showed pronounced tumor growth inhibition in the two mutant models, with significant tumor regression being achieved in each case while having relatively little impact on the A431 wild type model. In addition, these data allowed us to build on the observation that approximately 6 h cover over the free cell IC_{50} translated into both meaningful and prolonged in vivo PD biomarker modulation as well as substantial disease model efficacy (based on a range of additional compounds, data not shown).

With these highly encouraging in vivo data in hand, we elected to more fully characterize the pharmacokinetic properties of these compounds in species other than mice, and this information is captured in Table 7. In vivo clearance in rodents was moderate to high, and at low doses (5 mg/kg) oral bioavailability was low. Upon increasing dose however (>50 mg/kg), substantial oral levels could be obtained, and we postulated that this was probably occurring because of saturation of clearance mechanisms. However, dog pharmacokinetic profiling revealed medium clearance and generally good oral bioavailability.

Clearly the incorporation of the three basic side chains described above in **20**, **21**, and **22** combined with the migration of the base from the acrylamide had brought significant benefits relative to the start point **5**, and we proposed that this advance in SAR understanding might be applicable to some degree to the previously described indole analogues such as **9**. Although we

dx.doi.org/10.1021/jm500973a | J. Med. Chem. XXXX, XXX, XXX−XXX

Table 3. Structures and Selected Properties of Compounds 20, 21, and 22

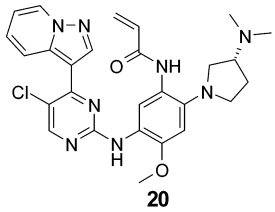

20

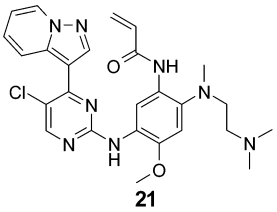

21

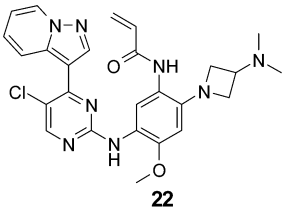

22

	20	21	22
DM cell IC_{50} (nM)	2	0.6	4
AM cell IC_{50} (nM)	16	2	21
WT cell IC_{50} (nM)	357	145	938
DM[a] antiproliferative cell GI_{50} (nM)	7	3	17
AM[a] antiproliferative cell GI_{50} (nM)	10	4	19
WT[a] antiproliferative cell GI_{50} (nM)	384	180	846
log $D_{7.4}$	3.1	2.8	3.3
LLE (DM cell)[b]	5.6	6.4	5.1
min sol. pH 7.4 (μM)	28 (Xtl)	222 (Xtl)	43 (Xtl)
rat % free[b]	7.1	6.4	5.1
human % free	2.7	3.2	2.5
nude mouse % free	7.8	3.2	5.0
rat Heps Cl_{int} [(μL/min)/(10^6 cells)]	20	59	27
human Heps Cl_{int} [(μL/min)/(10^6 cells)]	<3	14	5.2
mouse Heps Cl_{int} [(μL/min)/(10^6 cells)]	19	60	22
hERG IC_{50} (μM)	5.6	6.7	4.0
IGF1R (enz) IC_{50} (μM)	0.007	0.006	0.026
GSH mean $t_{1/2}$ (min)	140	90	257
pK_a (measured)	8.1	9	7.2
kinase panel[9a] hits (>90% inhibition at 1 μM)	IGF1R (98%)	IGF1R (97%)	IGF1R (97%)
	INSR (98%)	INSR (99%)	INSR (98%)

[a]Double mutant (DM) cell line: H1975. Activating mutant (AM) cell line: PC9. Wild type (WT) cell line: Calu3. [b]Plasma protein binding was assessed by equilibrium dialysis in the appropriate species at 37 °C in 10% plasma and extrapolated to100% with a single site binding model. Free and bound concentrations were quantified by LCMS.

Scheme 2. General Synthesis of Basic Side Chain Compounds 20, 21, and 22[a]

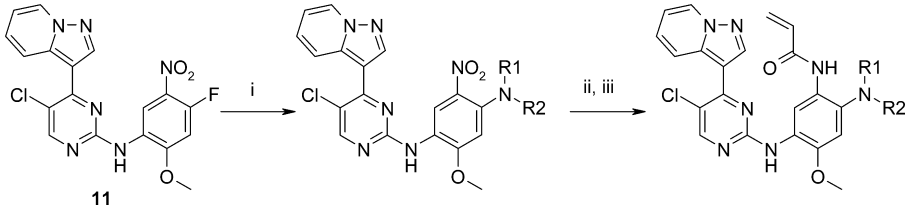

11

[a]Reagents and conditions: (i) R_1R_2NH, DIPEA, DMA, 85−100 °C; (ii) iron, NH_4Cl, EtOH, water, 100 °C; (iii) acryloyl chloride, DIPEA, DCM, −15 to 0 °C.

had previously moved away from the indole headgroup because of its more modest oral PK properties (vide supra) and smaller wild type margin relative to the pyrazolopyridine,[6] the enhanced potency available from this novel basic side chain SAR combined with the synthetic diversity handle offered by the indole N-H prompted us to re-examine this subseries. Thus, we decided to explore a matrix of compounds where we would incorporate favored groups at the 4 and 5 positions of the pyrimidine core with the newly identified basic side chain SAR (vide supra). Leading examples from this work are shown in Table 8. It should be noted that in addition to varying R1 and R2 as depicted in Table 8, additional examples were also prepared where the basic side chain was replaced with amines such as those in **22** and **20**, but none of these offered the levels of potency afforded by the *N,N,N′*-trimethylethylenediamine.

It can be seen that incorporation of the newly identified basic side chains delivered high cellular potency across all the examples shown (Table 8). The presence or indeed absence of a substituent at the 5-position of the pyrimidine ring also had a differential effect on double mutant potency, IGF1R potency, and hERG binding.

From Table 8 and the matched pair analysis in Figure 7, it is apparent that a 5-substituent has a beneficial impact on double mutant cell potency, possibly driven by interaction with the methionine gatekeeper residue, although in the case of the more polar cyano 5-substituent, the conformational effect on the indole group may also play a role. A similar trend is observed for IGF1R potency, again perhaps driven by this kinase's methionine gatekeeper, although it should be noted that the potency increase imparted by the 5-Cl is of a greater magnitude for IGF1R than any of the EGFR mutants or wild type receptor. Potency against

dx.doi.org/10.1021/jm500973a | J. Med. Chem. XXXX, XXX, XXX−XXX

Scheme 3. General Synthesis of Indole Compounds 23−27[a]

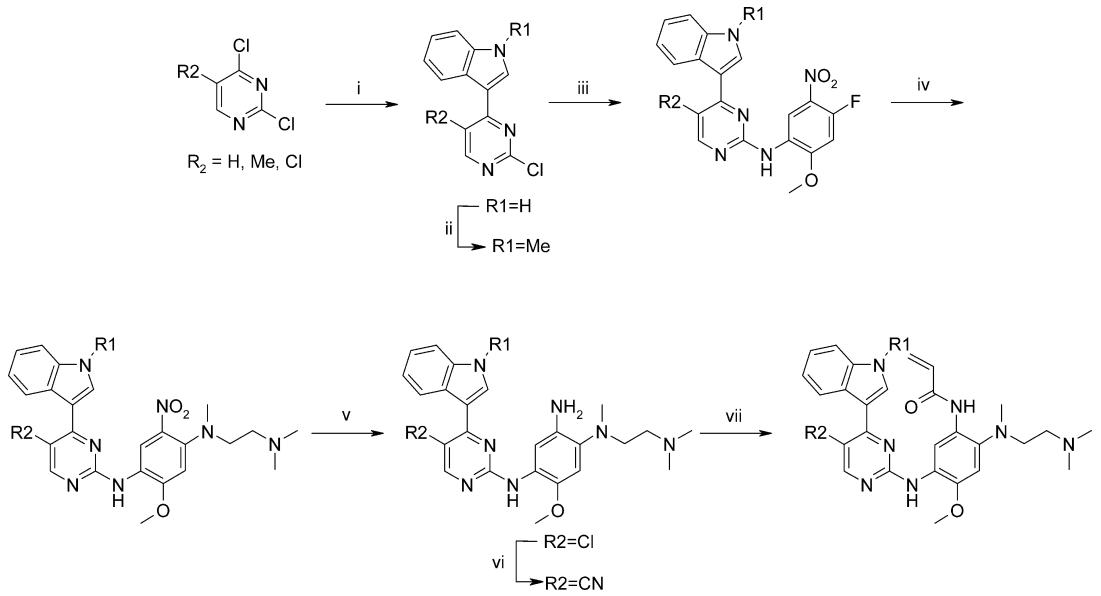

[a]Reagents and conditions: (i) MeMgBr (1 equiv, 3.2 M in 2-methyl THF), indole (1 equiv), THF, 0 °C → 60 °C; (ii) sodium hydride (1.05 equiv), methyl iodide (1.05 equiv), THF, 0 °C; (iii) 4-fluoro-2-methoxy-5-nitroaniline (1.05 equiv), tosic acid (1.1 equiv), 2-pentanol, 125 °C; (iv) *N*,*N*,*N*′-trimethylethane-1,2-diamine (2.2 equiv), DMA, 140 °C; (v) iron (3 equiv), ammonium chloride (0.7 equiv), EtOH, water, 100 °C; (vi) $Zn(CN)_2$ (0.6 equiv), zinc (0.1 equiv), tris(dibenzylideneacetone)dipalladium(0) (0.1 equiv), dicyclohexyl(2′,4′,6′-triisopropylbiphenyl-2-yl)phosphine (XPhos) (0.2 equiv), DMA, 95 °C; (vii) acryloyl chloride (1 M, THF, 1 equiv), DIPEA (1.1 equiv), THF, 0 °C.

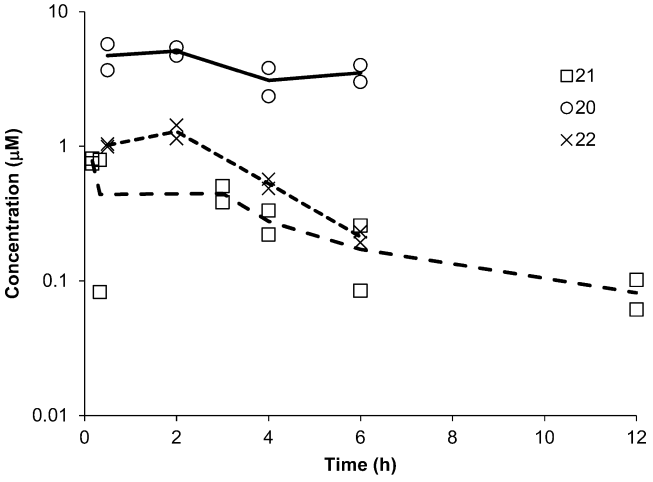

Figure 3. Mouse plasma concentration data following a 50 mg/kg oral dose of compound **20**, a 10 mg/kg oral dose of compound **21**, and a 10 mg/kg oral dose of compound **22**. Data points shown are concentrations from individual animals with mean values being represented by lines.

Table 4. Mouse Plasma C_{max} Concentration Data after a 50 mg/kg Oral Dose of Compound 20 and a 10 mg/kg dose of 21 and 22

compd	C_{max} (μM)	free C_{max} (μM)	free cover over DM cell IC_{50}	free cover over AM cell IC_{50}	free cover over WT cell IC_{50}
20	5.1	0.40	200	25	1.1
21	0.78	0.025	42	12	0.17
22	1.3	0.065	16	3	0.06

the activating mutant (data not shown) and wild type forms of the receptor was also increased, and the hERG potency for the compounds also followed a similar trend, although this is more difficult to rationalize. The presence or absence of a methyl group

Table 5. % Inhibition of p-EGFR (Measured by R&D Systems ELISA Kits, Not Site Specific and Expressed as Ratio of Phosphorylated/Total) in Mice Bearing PC9 Tumors after 10 mg/kg Oral Dose of Compounds 20, 21, and 22[a]

compd	1 h	6 h	16 h	24 h	30 h
20		76*		68*	
21	30	83***	60**	38	10
22	57**	85**	52*	19	

[a]Statistical significance (*p* values) was calculated by comparing compound treated and vehicle groups using a two-tailed *t*-test, unequal variance. *p* values are indicated as follows: (*) <0.05, (**) <0.01, (***) <0.001. See Supporting Information for further detail.

Table 6. % Inhibition of p-EGFR in Mice Bearing H1975 Tumors after 10 mg/kg Oral Dose of Compounds 20, 21, and 22[a]

compd	1 h	6 h	16 h	24 h	30 h
20		94***		88***	
21	89***	100***	94**	93**	80***
22	37	99***	82***	79***	50**

[a]*p* values are indicated as follows: (*) <0.05, (**) <0.01, (***) <0.001.

on the indole 1-position nitrogen also had interesting effects. Again, examination of Table 8 and matched pair analysis shown in Figure 8 reveals that the removal of the methyl group does appear to drive increased cell potency against all three EGF receptors (only double mutant shown graphically), with hERG potency having no discernible trend. The picture for IGF1R potency is more straightforward, with the NH indole analogues showing increased IGF1R potency. The SAR for wild type selectivity is also shown, with double mutant selectivity over wild type showing a statistically significant trend to be greater in the N-methylated compounds, whereas the N-Me indole examples when examined as a whole showed no statistically significant

dx.doi.org/10.1021/jm500973a | J. Med. Chem. XXXX, XXX, XXX−XXX

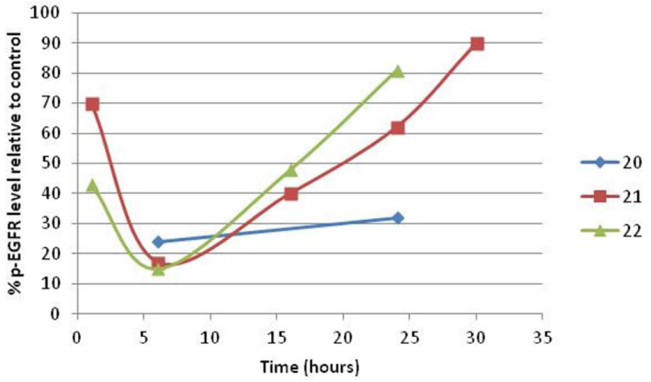

Figure 4. p-EGFR inhibition time course profile in PC9 (sensitizing mutant) xenograft bearing mice following 10 mg/kg oral dose of compounds **20**, **21**, and **22**.

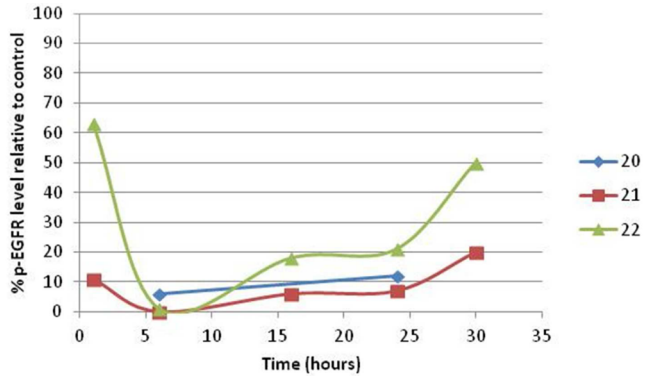

Figure 5. p-EGFR inhibition time course profile in H1975 (double mutant) xenograft bearing mice following 10 mg/kg oral dose of compounds **20**, **21**, and **22**.

activating mutant selectivity over the wild type form of the receptor when compared with their NH matched pairs. When profiled in the Millipore kinase selectivity panel,[9b] it became evident that for the two 5-H compounds tested, in addition to reducing IGF1R and INSR activity, we had also maintained the high selectivity of our above-described inhibitors.

Table 7. In Vivo Pharmacokinetic Parameters for 20, 21, and 22[a]

	20	21	22
rat[b] iv CL (mL min^{-1} kg^{-1})	22	60	59
rat HW po F (%)	13	10	24
mouse iv CL (mL min^{-1} kg^{-1})	77	17	106
mouse po F (%)	31	13	57
dog iv CL_p (mL min^{-1} kg^{-1})	16	25	7
dog po F (%)	67	30	56

[a]Rat oral bioavailability is from a 5 mg/kg dose. Mouse oral bioavailability is from a 10 mg/kg dose. Dog oral bioavailability is from a 5 mg/kg dose. [b]Han Wistar strain.

By examination of the data for this matrix of compounds in more detail, it can be seen that while very attractive, the profiles of most of the compounds were broadly similar to the earlier examples **20**, **21**, and **22** described above. Given the wealth of available attractive options, additional candidate compounds would need to offer something quite different from those already selected to proceed further. Compound **8** demonstrated improved rat PK, reduced hERG affinity, and improved IGF1R margins relative to the previously described compounds, and so this compound was selected for further investigation. Compound **8** also offered an additional degree of broader chemical and profile diversity when compared to the previously described lead compounds. Upon dosing **8** in our three efficacy models, we observed comparable efficacy at relatively low doses (10 mg kg^{-1} day^{-1}, Figure 9). Intriguingly, excellent efficacy was also observed when **8** was dosed at 5 mg kg^{-1} day^{-1} and this unprecedented level of activity combined with its previously mentioned attractive attributes added to our interest in this compound, despite the slightly lower wild type selectivity relative to **20**, **21**, and **22**. Given our earlier free cover model, it seems difficult to explain how this level of efficacy could be achieved with the relatively modest exposure achieved with **8** (free C_{max} = 13 nM, 0.9-fold free cover over DM cell IC_{50}), but further understanding did become apparent with additional studies (vide infra).

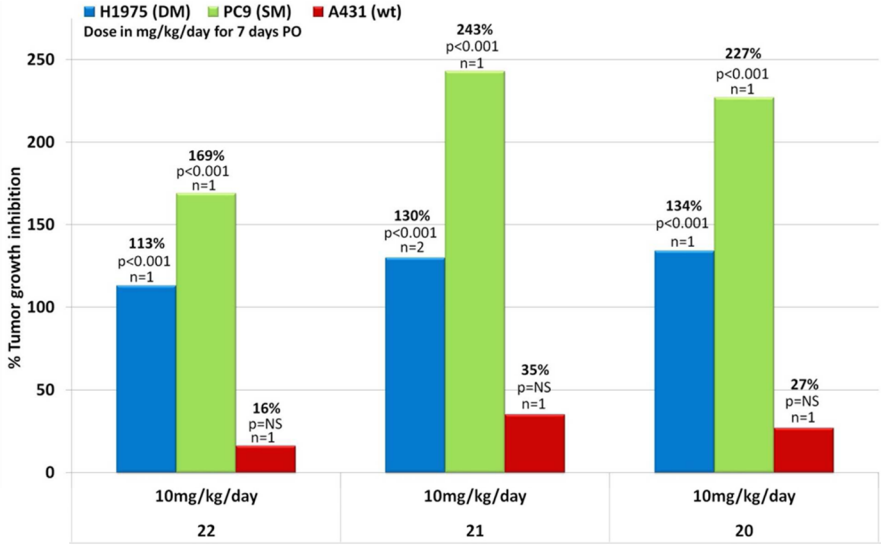

Figure 6. In vivo efficacy of **22**, **21**, and **20** when dosed orally in tumor bearing immune compromised mice at 10 mg kg^{-1} day^{-1} q.d. H1975 efficacy is represented in blue, with PC9 data in green and A431 in red. Statistical significance (p values) was calculated by comparing compound treated and vehicle groups using a one-tailed t test. "NS" indicates % TGI was not significant from vehicle.

dx.doi.org/10.1021/jm500973a | J. Med. Chem. XXXX, XXX, XXX−XXX

Table 8. Structure and Selected Data for Indole Compounds 23−27

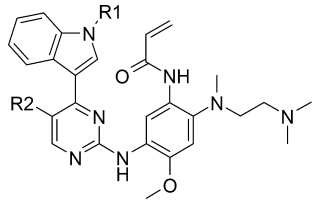

	23	24	25	26	8	27
R1/R2	Me/CN	Me/Cl	H/Cl	Me/Me	Me/H	H/H
DM cell IC_{50} (nM)	0.9	2	0.2	1	15	2
AM cell IC_{50} (nM)	1	2	0.6	2	17	2
WT cell IC_{50} (nM)	46	58	11	71	480	33
DM antiproliferative cell GI_{50} (nM)	2 (n = 1)	4 (n = 1)	2 (n = 1)	4 (n = 1)	24	16
AM antiproliferative cell GI_{50} (nM)	0.8 (n = 1)	3 (n = 1)	2 (n = 1)	2 (n = 1)	23	21
WT antiproliferative cell GI_{50} (nM)	101 (n = 1)	192 (n = 1)	144 (n = 1)	970 (n = 1)	264	58
IGF1R IC_{50} (nM)	38 (n = 1)	40 (n = 1)	7 (n = 1)	196 (n = 1)	2900	263
hERG IC_{50} (μM)	4.3	7.4	14.8	15.6	16.2	17.5
log $D_{7.4}$	2.7	3.3	3.3	2.8	3.4	2.9
min sol. pH 7.4 (μM)	57	759	75	576	7	79
rat HW % free	11		7.5		3.2	16
human % free	8.9	2.3	3.6	7.5	2.9	7.5
mouse % free					3.4	13.4
rat Heps Cl_{int} [(μL/min)/(10^6cells)]			88		27	27
human Heps Cl_{int} [(μL/min)/(10^6 cells)]	10	10	<3	5.6	3.4	<3
rat HW iv Cl (mL min^{-1} kg^{-1})	62	27	12		45	
rat HW po F (%)	6	7	1		45	
mouse AUC/C_{max} (μM·h/μM), 10 mg/kg po	0.28/0.11	1.3/0.31	3.3/1.2	0/0	1.4/0.38	0.203/0.047
GSH mean $t_{1/2}$ (min)			136	123	121	191

With a selection of potent, wild type selective and efficacious compounds in hand, we investigated the in vivo toxicological profile of the most favored examples. The in vitro kinase selectivity testing had revealed a desirable selectivity profile albeit with inhibition of IGF1R and INSR as common hits. With this observation in mind, we designed bespoke rat toxicology studies to explore whether reversible inhibition of IGF1R-INSR would lead to hyperglycemia or impaired insulin signaling in vivo. Rats received a single oral dose of 200 mg/kg of each compound with assessment of blood glucose and insulin concentrations over a 24 h period (see Supporting Information). While all compounds were tolerated well, a single oral dose of **21** and **20** led to marked hyperglycemia and hyperinsulinemia (Figures 10 and 11). At the same dose, **22** did not cause significant changes in blood glucose levels, but insulin levels were clearly increased, consistent with insulin being a more sensitive marker for perturbation of the glucose/insulin axis. In contrast, **8** did not impact measured levels of glucose or insulin. This is consistent with the observation that **8** was the only compound out of the four leading candidates that did not inhibit IGF1R (Table 8) or INSR (Table 9) with high potency.

Assessment of the toxicokinetics of the four compounds at 200 mg/kg in this study revealed that the free exposure of **8** was lower than the other three compounds (Table 9). Compounds **20**, **21**, and **22** were subsequently administered orally at the lower dose of 50 mg/kg, and despite a similar free exposure to compound **8**, they were still associated with hyperinsulinemia. The observed hyperinsulinemia with **20**, **21**, and **22** at both doses tested was consistent with the free exposure (C_{ave}) giving cover over the INSR IC_{50} (Table 9). In contrast, compound **8** did not provide cover over the INSR IC_{50}, and furthermore at a dose of 200 mg/kg the INSR IC_{50} was approximately 50-fold higher than the free exposure (C_{ave}). For compound **8**, pharmacological cover over the INSR IC_{50} and perturbation of the insulin−glucose axis was considered extremely unlikely.

Although IGF1R inhibitors have been studied clinically in an oncology setting, hyperglycemia can be dose limiting.[10] Inhibition of IGF1R and INSR signaling and its associated pharmacology had the potential to limit maximal tolerated doses in the NSCLC EGFR sensitive patient setting. Furthermore, it could affect patient exclusion criteria and require additional monitoring during clinical trials. In light of these findings it was decided to focus remaining efforts on **8** and **22** which had no or minimal effects on the IGF1R−INSR axis, respectively.

We subsequently performed a preliminary cardiovascular safety evaluation of the final two lead compounds. The compounds were assessed in an in vivo guinea pig model[15] to explore the effect of the compounds on hemodynamic, ECG, and contractility paramaters. Comparison of the cardiovascular profile revealed a major difference in the compounds with respect to QT prolongation. In contrast to **8**, **22** was associated with a pronounced QT prolongation at free C_{max} concentrations less than 30-fold predicted human free C_{max}. These data were consistent with the in vitro data for both compounds with **22** clearly having a higher affinity for the hERG ion channel than **8** (Ionworks hERG IC_{50} for **22** and **8** is 4.3 and 16.2 μM, respectively). In view of the data package as a whole, **8** was considered to have a very desirable profile and was ultimately selected as a clinical candidate. The selectivity profile of **8** as determined in the Millipore kinase panel[16] of 270 kinases is shown in Figure 12 (complete data are available in the Supporting Information), and it can be seen that the compound displays a good overall profile with the majority of more active hits being other tyrosine kinases. Compound **8** both exploits and illustrates the SAR we have discussed

dx.doi.org/10.1021/jm500973a | J. Med. Chem. XXXX, XXX, XXX−XXX

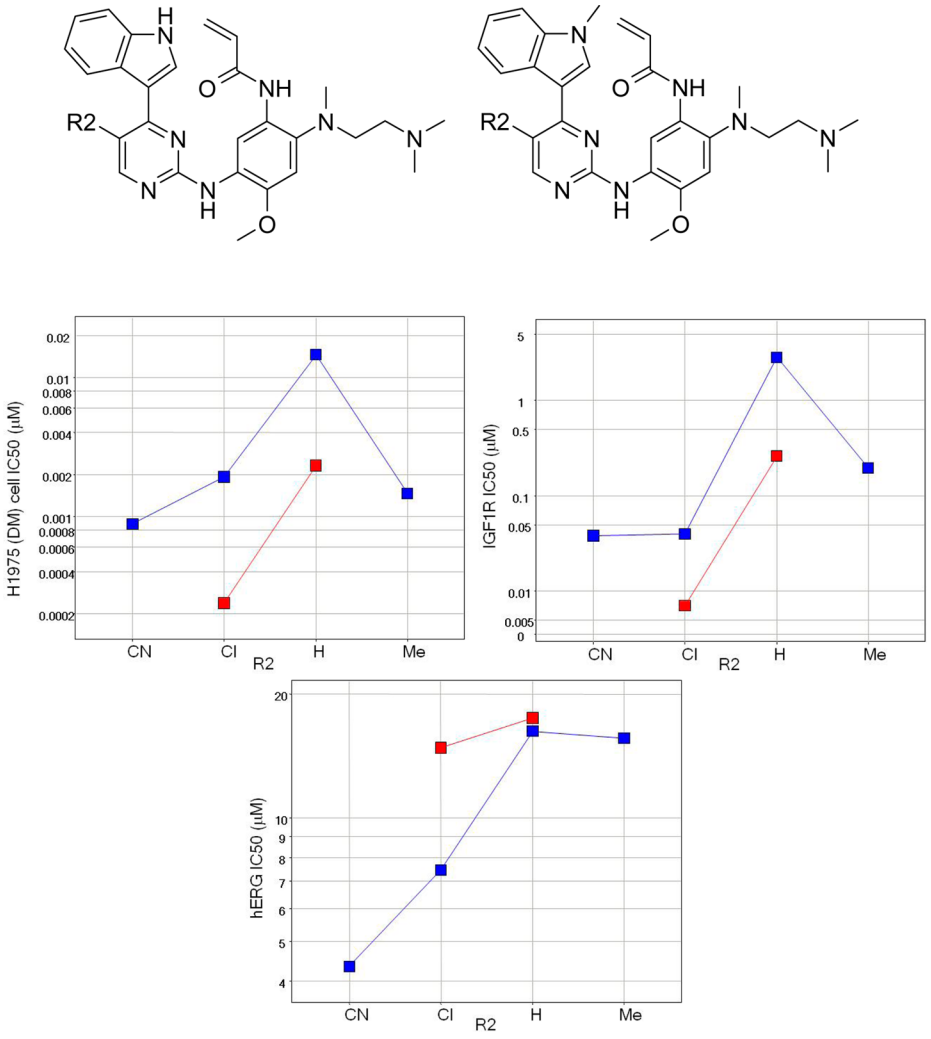

Figure 7. Pyrimidine 5-substituent analysis. N-H indoles appear in red, with N-Me indoles in blue.

above. The addition of the methyl group to the indole increases WT selectivity and reduces IGF1R potency (Figure 8). Removing the 5-Cl group from the monoanilinopyrimidine scaffold reduces the IGF1R potency, WT selectivity, and to a lesser extent DM potency, but the last can be recovered by employing the inherently more potent indole rather than pyrazolopyridine headgroup, and indole N−H alkylation can be used to drive WT selectivity.

Although we are yet to obtain an X-ray crystal structure of **8** bound to the EGFR T790M mutant, we were able to employ a published structure (PDB code 3IKA)[7] to model the binding mode of the inhibitor, and this is shown in Figure 13. Notable features include the covalent bond formed to C797, the hinge interaction at M793, and the orientation of the indole.

Having selected **8** for further development, we wished to further understand its metabolic fate in vivo. Previously, when looking at in vivo metabolism in rat bile samples, little had been evident apart from glutathione conjugation to the acrylamide portion of the molecule. In contrast, when in vivo plasma samples from rat and mouse were examined in more detail, it became evident that loss of the indole *N*-methyl group was occurring, leading to small quantities of the metabolite **27** (Figure 14). In addition, dealkylation was also seen to occur to a small extent in the *N*,*N*,*N*′-trimethylethylenediamine side chain of **8**, yielding **28** (Figure 14). A small amount of the side chain *N*-oxide was also evident at low levels.

Shown in Figure 15 are the total levels for **8**, **27**, and **28** over a 12 h period following a 25 mg/kg oral dose in the nude mouse. As can be seen from Table 10, **28** appeared to offer a broadly similar potency and selectivity profile to the parent compound. In contrast, we had previously prepared and profiled **27** (see Table 8), but despite its impressive double and activating mutant potency, we had not progressed the compound further, partly because of its modest in vitro wild type margin. In addition, oral dosing in the mouse led to only modest levels of exposure and low levels of free cover over the cellular IC_{50} values. Nevertheless, we were now faced with the intriguing prospect that a degree of the observed efficacy in vivo for **8** was actually driven by the metabolite **27**.

While **27** is present at lower concentrations in vivo than **8**, its higher cellular potency and lower protein binding equate to broadly similar free cover in vivo. A number of experiments were undertaken to try and establish the in vivo efficacy of **8** in the absence of **27**. These included co-dosing mice with **8** and the pan cytochrome P-450 inhibitor benzotriazol-1-amine (ABT)[17,18] in an attempt to reduce oxidative metabolism of the indole *N*-methyl group to give **27**. In addition, we undertook the preparation of an isotopically labeled version of **8**, where the indole *N*-methyl group was replaced by the $^{13}CD_3$ equivalent. Our hypothesis here was that the kinetic isotope effect[19] might slow the deuterium atom extraction process relative to the

dx.doi.org/10.1021/jm500973a | J. Med. Chem. XXXX, XXX, XXX−XXX

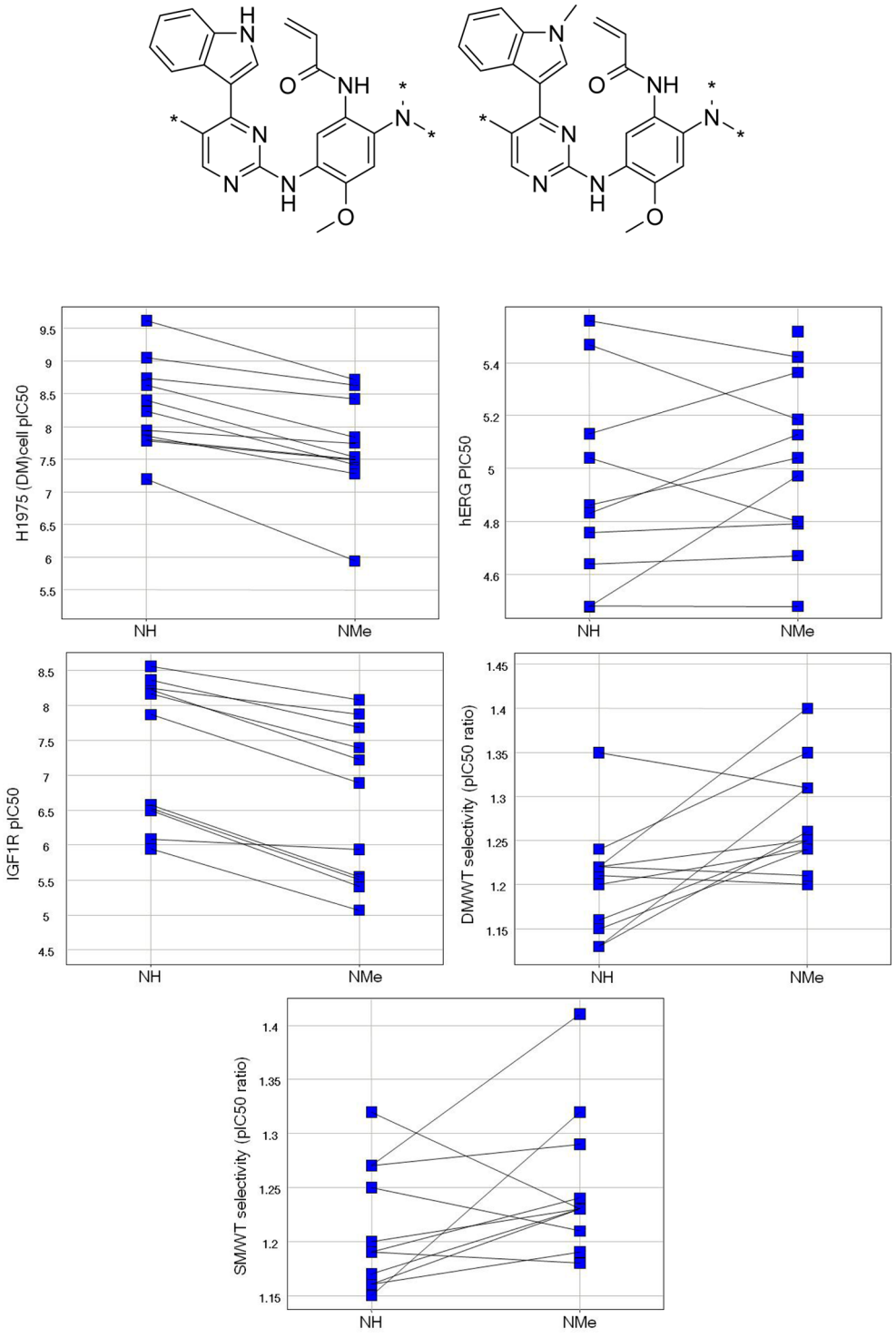

Figure 8. Matched pair analyses for N-H-indole and N-Me examples. Each marker represents an individual compound matching the substructure shown. Lines connect exact structural matches (∗ = positions of variation). Top left mean pIC_{50} difference is 0.61 (SE = 0.1, n = 11). Top right mean pIC_{50} difference is 0.06 (SE = 0.078, n = 11). Middle left mean pIC_{50} difference is 0.77 (SE = 0.09, n = 11). Middle right mean pIC_{50} difference is 0.072 (SE = 0.02, n = 11). Bottom mean pIC_{50} difference is 0.04 (SE = 0.02, n = 11).

corresponding hydrogen atom reaction and thus suppress formation of **27**, but neither of these measures were able to prevent the in vivo formation of **27** to an extent that its contribution to efficacy could be ignored.

In order to try and understand the implications of the presence of the metabolite **27** in vivo, we elected to dose **27** in all three of the previously described efficacy models. Examination of the outcome from these studies (Figure 16) showed that while substantial double and activating mutant efficacy is apparent, the level of wild type efficacy was also significant, reflecting the narrower in vitro margin as predicted from the in vitro cellular potency. It is also noteworthy that in the case of **27**, only very modest cover over the free cell IC_{50} is needed to achieve significant efficacy, in contrast to other compounds profiled in this

dx.doi.org/10.1021/jm500973a | J. Med. Chem. XXXX, XXX, XXX−XXX

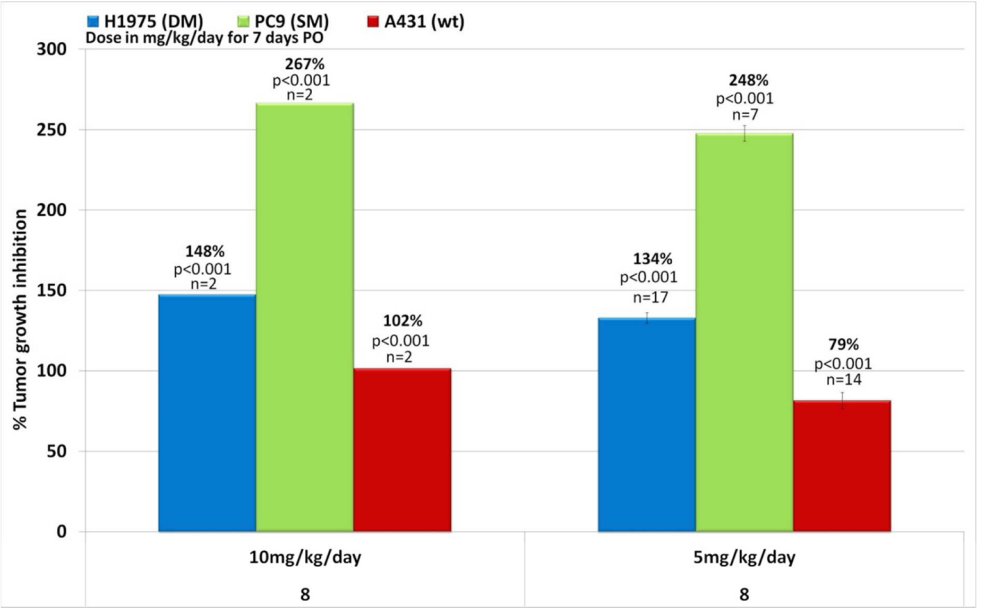

Figure 9. In vivo xenograft activity of **8** when dosed orally in tumor bearing immune compromised mice at 10 and 5 mg/kg q.d.

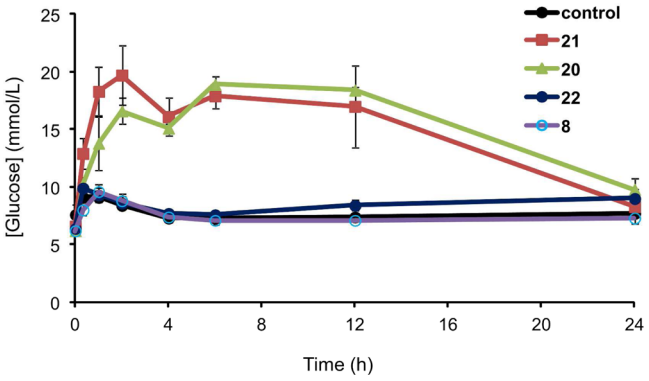

Figure 10. Compound effects of blood glucose levels in the rat following a single 200 mg/kg oral dose of compounds **20**, **21**, **22**, and **8**.

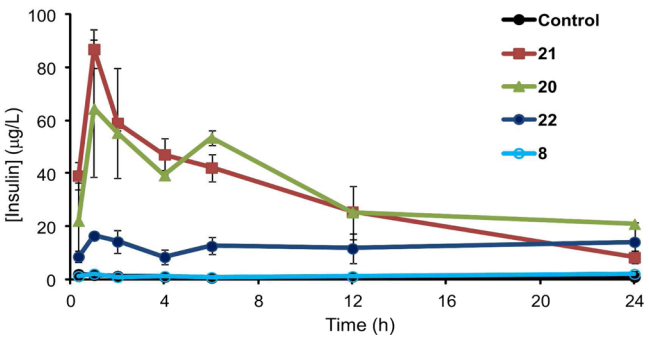

Figure 11. Compound effects of blood insulin levels in the rat following a single 200 mg/kg oral dose of compounds **20**, **21**, **22**, and **8**.

way. This is also apparent for **8**, but the presence of **27** in vivo makes this observation simpler to rationalize.

Comparison of the efficacy profiles between the two compounds revealed significant differences, and while it is likely that **27** contributes to the observed in vivo efficacy of **8**, it does not appear to be the sole driver. It is apparent from Figure 16 that the efficacy profiles of **8** and **27** are quite different from both the reversible inhibitor gefitinib (**1**) and the irreversible compound

Table 9. Exposure, INSR Potency/Fold Cover, and Effects on Blood Insulin Levels in the Rat after a Single 200 or 50 mg/kg po Dose of Compounds 20, 21, 22 and a Single 200 mg/kg Dose of 8

compd	dose (mg/kg)	free C_{ave} over 24 h	INSR IC_{50} (μM)	free fold cover over INSR IC_{50}	mean insulin increase over 24 h
8	200	0.0169	0.912	0.018	1.1
20	200	0.1101	0.021	5.3	30.7
	50	0.0358		1.7	13.4
21	200	0.0575	0.009	6.2	33.7
	50	0.0277		3	9.5
22	200	0.102	0.035	2.9	9.5
	50	0.06		1.7	3.3

afatinib (**4**) and that mutant selective inhibitors **8** and **27** offer a superior efficacy profile than these earlier agents. Clearly, the extent of formation of **27** in human patients would be a pivotal piece of information, as while its absence could possibly compromise the efficacy of the agent, more substantial levels could potentially lead to diminished margins to EGFRi driven wild type toxicity. Predicting an efficacious dose in patients for this agent presented challenges in terms of the irreversible inhibition mode of action, but the contribution of the metabolite to PD and efficacy also complicated the picture. The full details of these studies will be reported elsewhere, but basing human PK estimations on a metabolite **27** formation rate of 25% of parent (formation of **28** could not be quantified in vitro), the predicted efficacious dose in patients based on data from the PC9 model was approximately 20 and 10 mg based on the H1975 model.

In silico modeling of human absorption[20] showed that **8** should not be solubility limited at clinically relevant doses with Fabs > 50% up to 330 mg. Although the free base properties of **8** were considered to offer a low biopharmaceutical risk, the mesylate salt was selected for further work because of manufacturing risks around the physical form of the free base. In vivo studies established that the pharmacokinetics of **8** mesylate were largely comparable to those of the free base.

dx.doi.org/10.1021/jm500973a | J. Med. Chem. XXXX, XXX, XXX−XXX

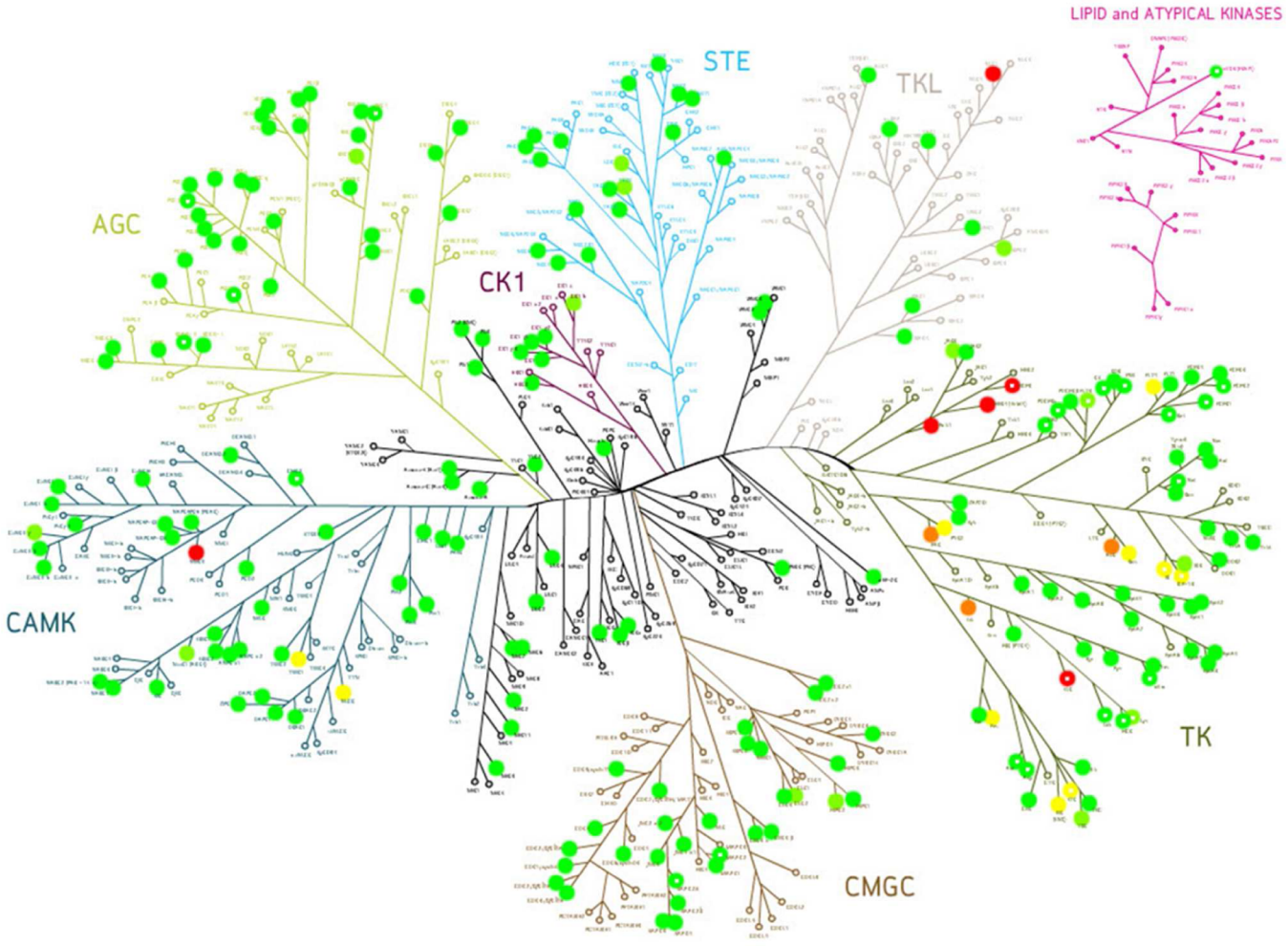

Figure 12. Millipore kinase selectivity profile for compound **8**. Colors are indicative of % inhibition at 1 μM as follows: dark green, 0−20% of control; light green, 20−40% of control; yellow, 40−60% of control; orange, 60−80% of control; red, 80−100% of control. Full % inhibition data are listed in the Supporting Information including IC_{50} data for those kinases with an analogous cysteine to C797.

The mesylate salt of **8** was first dosed in March 2013 to patients with EGFRm+ advanced NSCLC who had disease progression following treatment with an EGFR TKI (including **1** or **2**). On the basis of the work described above, the initial dose selected for oral administration to patients was set at 20 mg, once a day. Pharmacokinetic data from this cohort of six patients are shown below.[21] It can be seen that after a single dose, 7-day washout, and then 8 days of once daily dosing, exposure to **8**, **27**, and **28** was observed (Figure 17). It is also evident that the formation rate of the **27** metabolite is largely consistent with the predicted levels and that interpatient variability is low. Clearly these data discharge to some extent the above-mentioned potential risks around the presence or absence of **27**.

Clinical testing with **8** is ongoing, with encouraging initial efficacy seen in NSCLC patients. Data from two patients have recently been reported[21b,22] and are discussed here. Serial CT scans from two patients who received **8** at a 20 mg once daily dose are shown (Figures 18 and 19). Prior to commencing dosing, both patients' tumors were known to exhibit T790M mutations according to local testing, as well as EGFR sensitizing mutations. The first patient was a 57 year old East Asian female from South Korea diagnosed with stage IV EGFR mutant (ex 19 del) NSCLC in May 2011. Tumor shrinkage on treatment with **8** was 39.7% at RECIST 1.1 (response evaluation criteria in solid tumors)[23] scan 1, was 48.3% by scan 2 (Figure 18), remained at 48.3% at both scan 3 and scan 4, and was 51.7% at scan 5 (data not shown).

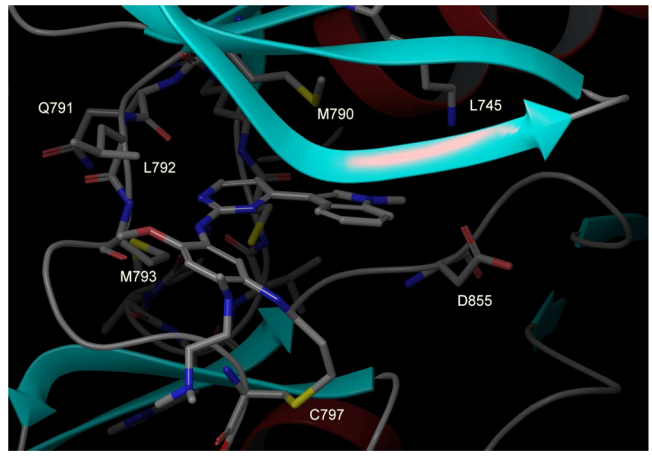

Figure 13. Modeled binding mode of compound (**8**). See Supporting Information for further details. Adapted by permission from the American Association for Cancer Research: Cross, D. A. E.; et al. AZD9291, an irreversible EGFR TKI, overcomes T790M-mediated resistance to EGFR inhibitors in lung cancer. *Cancer Discovery* **2014**, *4*, 1046−1061.[21b]

dx.doi.org/10.1021/jm500973a | *J. Med. Chem.* XXXX, XXX, XXX−XXX

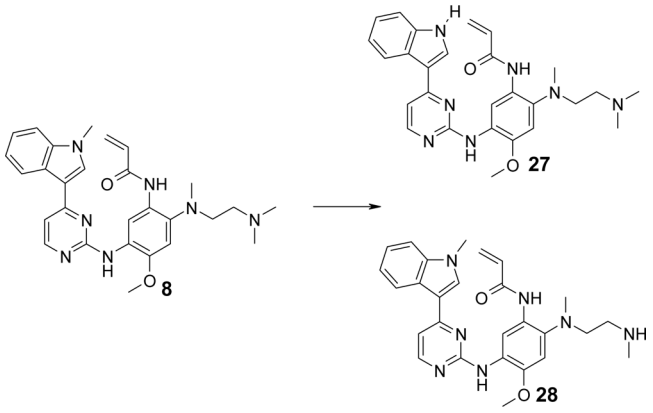

Figure 14. Compound **8** and identified circulating metabolites **27** and **28**.

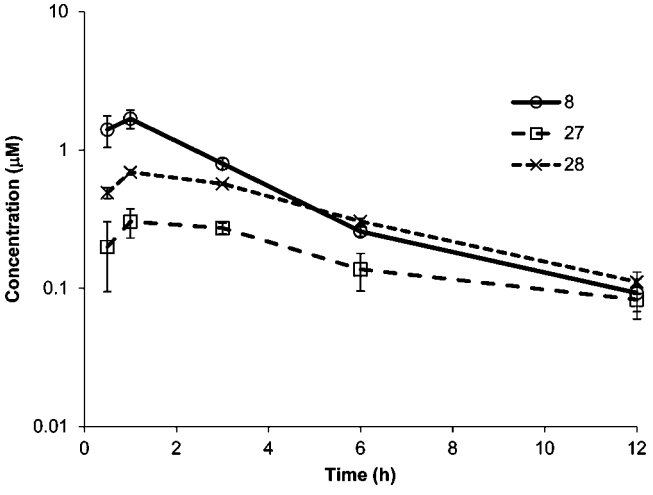

Figure 15. Total levels for **8**, **27**, and **28** over a 12 h period following a 25 mg/kg oral dose in the nude mouse. The markers are mean values ± SEM.

Table 10. Compound 28 in Vitro Profile

	28
DM cell IC_{50} (nM)	45
AM cell IC_{50} (nM)	26
WT cell IC_{50} (nM)	786
DM antiproliferative cell GI_{50} (nM)	19
AM antiproliferative cell GI_{50} (nM)	15
WT antiproliferative cell GI_{50} (nM)	537
IGF1R IC_{50} (μM)	1.6 (n = 1)
hERG IC_{50} (μM)	>33
log $D_{7.4}$	2.3
min sol. pH 7.4 (μM)	14
rat HW % free	2.3
human % free	3.9
mouse % free	1.05
rat Heps Cl_{int} [(μL/min)/(10^6 cells)]	50
human Heps Cl_{int} [(μL/min)/(10^6 cells)]	<3

The second subject[21b] was a 57 year old white female from the United Kingdom, diagnosed with stage IV lung adenocarcinoma in December 2010. At the cycle 1 day 15 assessments on **8**, the patient reported full resolution of pre-existing persistent nocturnal cough. Tumor shrinkage was 38% at RECIST 1.1 scan 1, 39.3% by scan 2, 56.7% by scan 3 (Figure 19), 62% by scan 4, and 59.3% by scan 5 (data not shown). By cycle 7 day 1, the patient reported significant improvement in pre-existing hair and eyelash abnormalities which had developed during the immediately prior gefitinib therapy. Both patients had a duration of response of approximately 9 months and were progression-free on 20 mg/day of compound **8** mesylate salt for approximately 11 months until disease progression by RECIST 1.1. Both patients continue to receive compound **8** treatment on study as per protocol, as they continue to derive clinical benefit according to their treating physicians. Consistent with **8** being less active against wild-type EGFR, in these two cases there

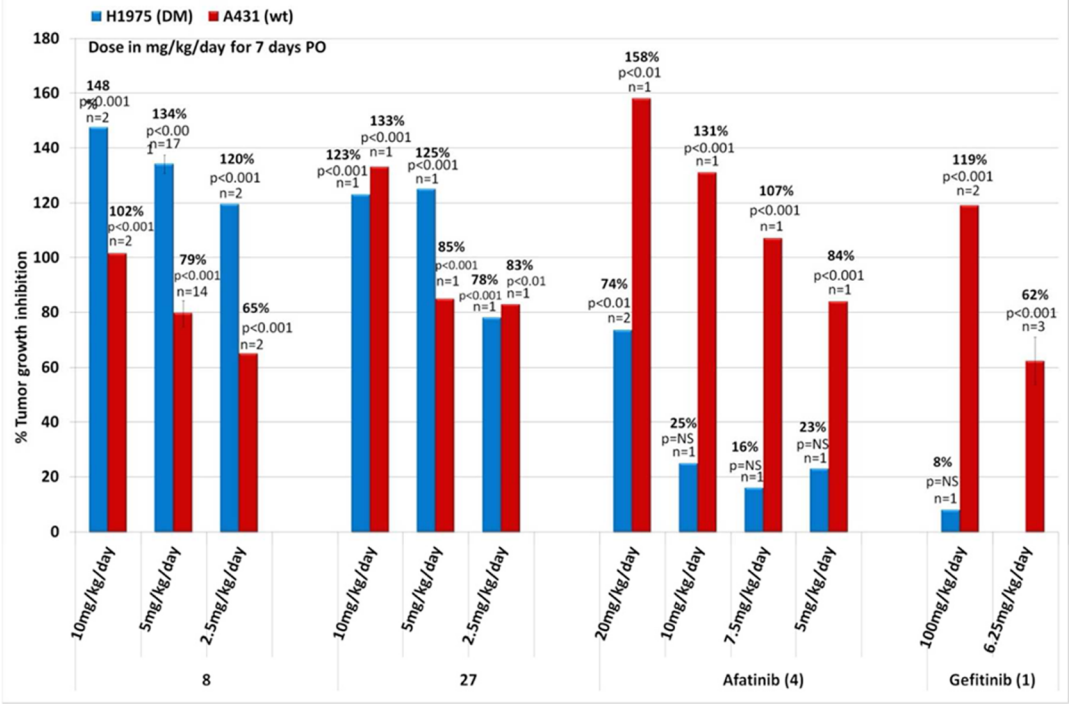

Figure 16. In vivo efficacy profiles (% tumor growth inhibition) of **8**, **27**, afatinib (**4**), and gefitinib (**1**).

dx.doi.org/10.1021/jm500973a | J. Med. Chem. XXXX, XXX, XXX−XXX

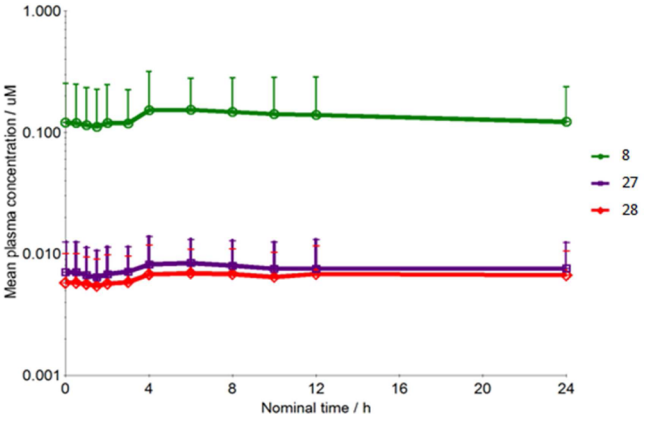

Figure 17. Preliminary plasma concentration versus time plots (mean + SD) of **8**, **27**, and **28** after 8 days of once daily 20 mg oral doses of **8** to patients with advanced EGFRm+ NSCLC in AURA phase 1 study (NCT01802632) (n = 6). Adapted by permission from the American Association for Cancer Research: Cross, D. A. E.; et al. AZD9291, an irreversible EGFR TKI, overcomes T790M-mediated resistance to EGFR inhibitors in lung cancer. *Cancer Discovery* **2014**, *4*, 1046−1061.[21b]

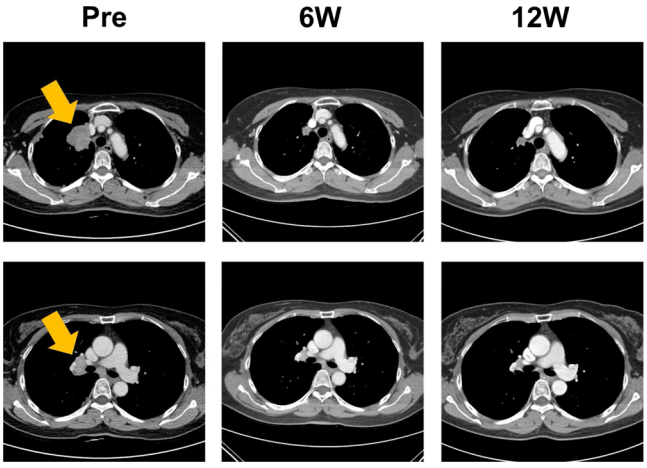

Figure 18. Serial computed tomography scans of the chest from patients before and after treatment with **8** in a phase I trial: images from a 57-year old Korean female patient diagnosed with stage IV non-small-cell lung cancer in May 2011. Adapted by permission from the American Association for Cancer Research: Cross, D. A. E.; et al. AZD9291, an irreversible EGFR TKI, overcomes T790M-mediated resistance to EGFR inhibitors in lung cancer. *Cancer Discovery* **2014**, *4*, 1046−1061.[21b]

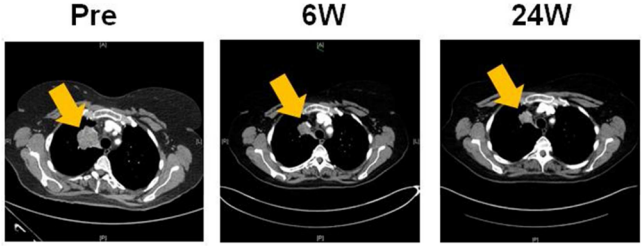

Figure 19. Serial computed tomography scans of the chest from patients before and after treatment with **8** in a phase I trial: images from a 57-year old British female never smoker diagnosed with stage IV lung adenocarcinoma in December 2010. Adapted by permission from the American Association for Cancer Research: Cross, D. A. E.; et al. AZD9291, an irreversible EGFR TKI, overcomes T790M-mediated resistance to EGFR inhibitors in lung cancer. *Cancer Discovery* **2014**, *4*, 1046−1061.[21b]

were no rash events and only one reported CTCAE (common terminology criteria for adverse events)[24] grade 1 diarrhea. No significant aberration of blood glucose levels were noted in either patient during the study.

CONCLUSION

We have described herein the evolution of a chemical series from lead selection to candidate nomination and the initial clinical findings with this novel agent. During the course of this work, a number of key challenges were addressed including off-target kinase selectivity and cardiovascular safety. Compound **8** offers a number of advantages over earlier EGFR TKI agents including high cellular potency, superior efficacy in relevant disease models, and selectivity over the wild type form of the receptor. The promising data package for **8** strongly supported its selection as a clinical candidate, and first dose in patients was achieved in March 2013. To date, encouraging and reproducible drug exposure has been achieved in humans, and of particular significance is the early evidence of tumor responses in patients who had previously progressed on earlier treatments, accompanied by good tolerability.[25] Additional safety, pharmacokinetic, and clinical data for **8** will be reported in due course.

EXPERIMENTAL SECTION

General. All solvents and chemical used were reagent grade. Purity and characterization of compounds were established by a combination of LCMS and NMR. LCMS spectra were obtained using a Waters liquid chromatography mass spectrometry system, where purity was determined by UV absorption at a wavelength of 254 nm, and the mass ion was determined by electrospray ionization (Micromass instrument). All test compounds were >95% pure as assessed by LCMS and ^{1}H NMR. ^{1}H NMR spectra were recorded using a Bruker Avance 400 FT spectrometer or via flow NMR process using an AVANCE 500 FT spectrometer and using DMSO-d_6 or $CDCl_3$ with the data expressed as chemical shifts in ppm from internal standard TMS. Preparative HPLC was performed on a Waters or Phenomenex column using decreasingly polar mixtures of water (containing 1% formic acid or 1% aqueous NH_4OH) and MeCN. Purification by column chromatography (FCC) was typically performed using silica gel (Merck 7734 grade), and solvent mixtures and gradients are recorded herein. Water present in compounds was quantified by Karl Fischer analysis. All reactions were performed under nitrogen unless otherwise stated. All IC_{50} data are quoted as geometric mean values, and statistical analysis is availble in the Supporting Information.

Synthesis of Representative Key Examples (Compounds 20, 21, 22, and 8). *N*-[5-[(5-Chloro-4-pyrazolo[1,5-*a*]pyridin-3-ylpyrimidin-2-yl)amino]-2-[(3*R*)-3-dimethylaminopyrrolidin-1-yl]-4-methoxyphenyl]prop-2-enamide (20). *5-Chloro-N-[4-[(3R)-3-dimethylaminopyrrolidin-1-yl]-2-methoxy-5-nitrophenyl]-4-pyrazolo-[1,5-a]pyridin-3-ylpyrimidin-2-amine.*

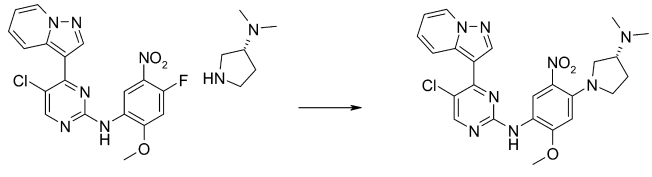

(*R*)-(+)-3-(Dimethylamino)pyrrolidine dihydrochloride (90 mg, 0.48 mmol) was added to a suspension of 5-chloro-*N*-(4-fluoro-2-methoxy-5-nitrophenyl)-4-pyrazolo[1,5-*a*]pyridin-3-ylpyrimidin-2-amine[6] (**11**, 200 mg, 0.48 mmol) and DIPEA (0.250 mL, 1.45 mmol) in DMA (3 mL). The mixture was heated at 140 °C in a microwave for 0.5 h. The mixture was diluted with MeOH and absorbed onto an SCX column, washed with MeOH, and eluted with 1:1 DCM/NH_3 in MeOH. Product-containing fractions were concentrated. The crude product was purified by flash silica chromatography, eluting with 1.5% 7 N NH_3/MeOH

dx.doi.org/10.1021/jm500973a | *J. Med. Chem.* XXXX, XXX, XXX−XXX

in DCM. Pure fractions were evaporated to dryness to afford 5-chloro-*N*-[4-[(3*R*)-3-dimethylaminopyrrolidin-1-yl]-2-methoxy-5-nitrophenyl]-4-pyrazolo[1,5-*a*]pyridin-3-ylpyrimidin-2-amine (149 mg, 61%) as an orange foam. ^{1}H NMR (400 MHz, DMSO, 21 °C) δ 1.76−1.89 (1H, m), 2.14−2.25 (7H, m), 2.69−2.84 (1H, m), 3.12−3.27 (3H, m), 3.41−3.53 (1H, m), 3.89 (3H, s), 6.56 (1H, s), 7.13 (1H, td), 7.26−7.38 (1H, m), 8.06 (1H, s), 8.40−8.43 (2H, m), 8.73 (1H, s), 8.85 (1H, d), 8.95 (1H, s); *m*/*z* (ES+) $(M + H)^+$ = 509.5.

N-(5-Chloro-4-pyrazolo[1,5-a]pyridin-3-ylpyrimidin-2-yl)-4-[(3R)-3-dimethylaminopyrrolidin-1-yl]-6-methoxybenzene-1,3-diamine.

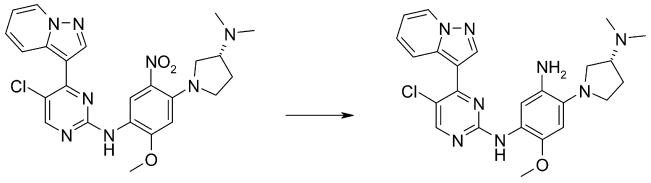

5-Chloro-*N*-[4-[(3*R*)-3-dimethylaminopyrrolidin-1-yl]-2-methoxy-5-nitrophenyl]-4-pyrazolo[1,5-*a*]pyridin-3-ylpyrimidin-2-amine (145 mg, 0.28 mmol), iron (95 mg, 1.71 mmol), and ammonium chloride (11.43 mg, 0.21 mmol) were heated in ethanol (6 mL) and water (2 mL) at reflux for 1.5 h. The mixture was cooled and concentrated. The residue was triturated in 10% MeOH/DCM (15 mL) for 15 min and filtered. The residues were retriturated with 10% MeOH/DCM (15 mL) and filtered. The combined filtrates were washed with brine, dried (Na_2SO_4), and concentrated. The crude product was purified by flash silica chromatography, eluting with 2% 7 N NH_3/MeOH in DCM. Pure fractions were evaporated to dryness to afford *N*-(5-chloro-4-pyrazolo-[1,5-*a*]pyridin-3-ylpyrimidin-2-yl)-4-[(3*R*)-3-dimethylaminopyrrolidin-1-yl]-6-methoxybenzene-1,3-diamine (112 mg, 82%) as a yellow gum. ^{1}H NMR (400 MHz, $CDCl_3$, 21 °C) δ 1.83−1.96 (1H, m), 2.08−2.23 (1H, m), 2.30 (6H, s), 2.82−2.92 (1H, m), 2.99−3.13 (2H, m), 3.17−3.28 (2H, m), 3.65 (2H, s), 3.84 (3H, s), 6.72 (1H, s), 6.96 (1H, td), 7.38 (1H, ddd), 7.52 (1H, s), 7.90 (1H, s), 8.36 (1H, s), 8.55−8.60 (1H, m), 8.65 (1H, dd), 8.94 (1H, s); *m*/*z* (ES+) $(M + H)^+$ = 479.5.

N-[5-[(5-Chloro-4-pyrazolo[1,5-a]pyridin-3-ylpyrimidin-2-yl)-amino]-2-[(3R)-3-dimethylaminopyrrolidin-1-yl]-4-methoxyphenyl]-prop-2-enamide.

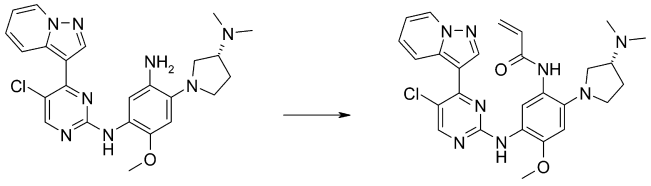

Acryloyl chloride (0.042 mL, 0.51 mmol) in DCM (1 mL) was added dropwise to *N*-(5-chloro-4-pyrazolo[1,5-*a*]pyridin-3-ylpyrimidin-2-yl)-4-[(3*R*)-3-dimethylaminopyrrolidin-1-yl]-6-methoxybenzene-1,3-diamine (245 mg, 0.51 mmol) and DIPEA (0.097 mL, 0.56 mmol) in DCM (10 mL), cooled in an ice/water bath. The mixture was stirred for 2 h and then washed with brine, dried (Na_2SO_4), and concentrated. The crude product was purified by flash silica chromatography, eluting with 2% 7 N NH_3/MeOH in DCM. Pure fractions were evaporated to dryness to give a foam. This was triturated with DCM/Et_2O and concentrated. The solid was triturated with Et_2O and filtered to afford *N*-[5-[(5-chloro-4-pyrazolo[1,5-*a*]pyridin-3-ylpyrimidin-2-yl)amino]-2-[(3*R*)-3-dimethylaminopyrrolidin-1-yl]-4-methoxyphenyl]prop-2-enamide (157 mg, 58%) as a yellow solid. ^{1}H NMR (400 MHz, DMSO, 22 °C) δ 1.68−1.83 (1H, m), 2.05−2.16 (1H, m), 2.18 (6H, s), 2.64−2.76 (1H, m), 3.18−3.29 (3H, m), 3.36−3.47 (1H, m), 3.77 (3H, s), 5.67 (1H, dd), 6.16 (1H, dd), 6.48 (1H, dd), 6.54 (1H, s), 7.12 (1H, t), 7.37 (1H, t), 7.43 (1H, s), 8.28−8.46 (2H, m), 8.55 (1H, s), 8.83 (1H, d), 8.94 (1H, s), 9.37 (1H, s); ^{13}C NMR (176 MHz, DMSO, 22 °C) δ 29.4, 43.8, 49.2, 54.8, 55.6, 65.1, 99.3, 107.1, 113.8, 114.2, 117.7, 119.0, 120.6, 125.5, 125.7, 126.9, 129.3, 131.9, 139.3, 142.8, 143.2, 151.5, 155.4, 157.8, 159.4. CHN analysis, $C_{27}H_{29}O_2N_8Cl$ requires C = 60.84%, H = 5.48%, N = 21.02%. Found: C = 60.7%, H = 5.6%, N = 21.0%. *m*/*z* (ES+) $(M + H)^+$ = 533.5. HRMS: $(M + H)^+ = C_{27}H_{30}O_2N_8Cl$ = 533.21747, found 533.21747.

***N*-[5-[(5-Chloro-4-pyrazolo[1,5-*a*]pyridin-3-ylpyrimidin-2-yl)-amino]-2-(2-dimethylaminoethylmethylamino)-4-methoxyphenyl]-prop-2-enamide (21).** *N-(5-Chloro-4-pyrazolo[1,5-a]pyridin-3-ylpyrimidin-2-yl)-N′-(2-dimethylaminoethyl)-2-methoxy-N′-methyl-5-nitrobenzene-1,4-diamine.*

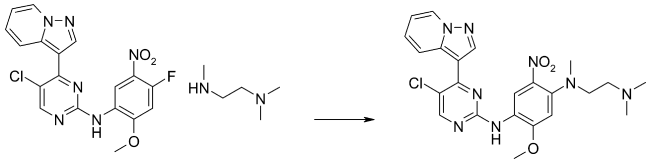

N,*N*,*N*′-Trimethylethylenediamine (0.188 mL, 1.45 mmol) was added to a suspension of 5-chloro-*N*-(4-fluoro-2-methoxy-5-nitrophenyl)-4-pyrazolo[1,5-*a*]pyridin-3-ylpyrimidin-2-amine (**11**, 500 mg, 1.21 mmol) and *N*-ethyldiisopropylamine (0.250 mL, 1.45 mmol) in DMA (5 mL). The mixture was heated at 140 °C in a microwave for 30 min. The mixture was diluted with MeOH and absorbed onto an SCX column, washed with MeOH, and eluted with 1:1 DCM/NH_3 in MeOH. Product containing fractions were evaporated to dryness to afford *N*-(5-chloro-4-pyrazolo[1,5-*a*]pyridin-3-ylpyrimidin-2-yl)-*N*′-(2-dimethylaminoethyl)-2-methoxy-*N*′-methyl-5-nitrobenzene-1,4-diamine (624 mg, 104%) as an orange solid. ^{1}H NMR (400 MHz, DMSO, 30 °C) δ 2.17 (6H, d), 2.89 (3H, d), 3.87−3.93 (3H, m), 6.84 (1H, s), 7.14 (1H, td), 7.31−7.38 (1H, m), 8.15 (1H, s), 8.39 (1H, d), 8.44 (1H, d), 8.69 (1H, s), 8.85 (1H, d), 8.95 (1H, s); *m*/*z* (ES+) $(M + H)^+$ = 497.

N4-(5-Chloro-4-pyrazolo[1,5-a]pyridin-3-ylpyrimidin-2-yl)-N1-(2-dimethylaminoethyl)-5-methoxy-N1-methylbenzene-1,2,4-triamine.

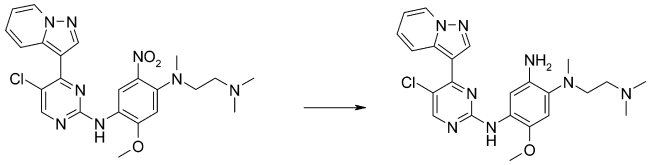

A solution of ammonium chloride (45.2 mg, 0.85 mmol) in water (10 mL) was added in one portion to a stirred mixture of *N*-(5-chloro-4-pyrazolo[1,5-*a*]pyridin-3-ylpyrimidin-2-yl)-*N*′-(2-dimethylaminoethyl)-2-methoxy-*N*′-methyl-5-nitrobenzene-1,4-diamine (600 mg, 1.21 mmol) and iron (405 mg, 7.24 mmol) in ethanol (30 mL). The resulting mixture was stirred at 105 °C for 3 h. The mixture was evaporated to dryness and the residue triturated with DMF (10 mL). The crude product was purified by ion exchange chromatography, using an SCX column. The desired product was eluted from the column using 0.35 M NH_3/MeOH/DCM, and pure fractions were evaporated to dryness to afford *N*4-(5-chloro-4-pyrazolo[1,5-*a*]pyridin-3-ylpyrimidin-2-yl)-*N*1-(2-dimethylaminoethyl)-5-methoxy-*N*1-methylbenzene-1,2,4-triamine (530 mg, 94%) as a brown gum. ^{1}H NMR (400 MHz, DMSO, 22 °C) δ 2.16 (6H, d), 2.38 (2H, t), 2.66 (3H, d), 2.92 (2H, t), 3.66 (3H, s), 4.60 (2H, s), 6.78 (1H, s), 6.92 (1H, s), 7.12 (1H, t), 7.27−7.4 (1H, m), 8.38 (1H, s), 8.43 (1H, d), 8.49 (1H, s), 8.83 (1H, d), 8.95 (1H, s); *m*/*z* (ES+) $(M + H)^+$ = 467.

N-[5-[(5-Chloro-4-pyrazolo[1,5-a]pyridin-3-ylpyrimidin-2-yl)-amino]-2-(2-dimethylaminoethylmethylamino)-4-methoxyphenyl]-prop-2-enamide.

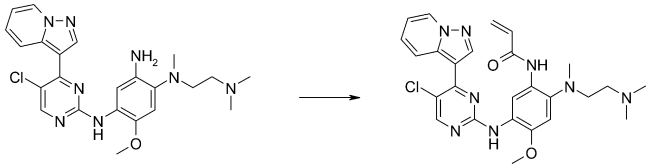

Acryloyl chloride (1.248 mL, 1M, THF, 1.25 mmol) was added dropwise to *N*4-(5-chloro-4-(pyrazolo[1,5-*a*]pyridin-3-yl)pyrimidin-2-yl)-*N*1-(2-(dimethylamino)ethyl)-5-methoxy-*N*1-methylbenzene-1,2,4-triamine (530 mg, 1.13 mmol) and DIPEA (0.244 mL, 1.36 mmol) in THF (20 mL) cooled to 0 °C. The resulting mixture was stirred at 0 °C for 2 h. The reaction mixture was evaporated to dryness and redissolved in DCM (100 mL) and washed sequentially with saturated

dx.doi.org/10.1021/jm500973a | J. Med. Chem. XXXX, XXX, XXX−XXX

$NaHCO_3$ (25 mL), water (25 mL), and saturated brine (25 mL). The organic layer was evaporated to afford crude product. The crude product was purified by flash silica chromatography, with elution gradient 0−20% 2 M NH_3/methanol in DCM. This gave product still containing impurities. The crude product was purified by flash silica chromatography, with elution gradient 0−20% MeOH in DCM. Pure fractions were evaporated to dryness to afford a brown gum. Again this showed impurities by LCMS. The crude product was purified by flash silica chromatography, with elution gradient 0−20% MeOH in DCM to yield *N*-[5-[(5-chloro-4-pyrazolo[1,5-*a*]pyridin-3-ylpyrimidin-2-yl)amino]-2-(2-dimethylaminoethylmethylamino)-4-methoxyphenyl]prop-2-enamide (191 mg, 32%) as a brown gum. Lyophilization from MeOH/water gave a brown semisolid. Trituration of the semisolid with ether followed by evaporation of the ether gave *N*-[5-[(5-chloro-4-pyrazolo-[1,5-*a*]pyridin-3-ylpyrimidin-2-yl)amino]-2-(2-dimethylaminoethyl-methylamino)-4-methoxyphenyl]prop-2-enamide (191 mg, 32%) as a pale yellow solid. ^{1}H NMR (400 MHz, $CDCl_3$, 22 °C) δ 2.28 (6H, s), 2.32 (2H, t), 2.71 (3H, s), 2.84−2.92 (2H, m), 3.87 (3H, s), 5.67 (1H, dd), 6.29 (1H, dd), 6.37 (1H, dd), 6.80 (1H, s), 6.89 (1H, td), 7.23−7.33 (1H, m), 7.46 (1H, s), 8.45 (1H, s), 8.52 (1H, d), 8.56 (1H, d), 8.94 (1H, s), 9.39 (1H, s), 10.09 (1H, s); ^{13}C NMR (176 MHz, DMSO, 22 °C) δ 29.4, 41.8, 44.9, 45.0, 55.7, 56.7, 105.8, 106.9, 113.8, 114.3, 117.7, 120.3, 124.0, 126.2, 127.1, 129.0, 132.0, 139.0, 140.0, 143.0, 148.9, 155.3, 157.5, 158.9. CHN analysis, $C_{26}H_{29}N_8O_2Cl$ requires C = 59.94%, H = 5.61%, N = 21.51%. Found: C = 60.2%, H = 5.7%, N = 21.7%; *m*/*z* (ES+) $(M + H)^+$ = 521.29; HRMS: $(M + H)^+ = C_{26}H_{30}N_8O_2Cl$ = 521.217 47, found 521.217 59.

N-[5-[(5-Chloro-4-pyrazolo[1,5-*a*]pyridin-3-ylpyrimidin-2-yl)-amino]-2-(3-dimethylaminoazetidin-1-yl)-4-methoxyphenyl]-prop-2-enamide (22). *5-Chloro-N-[4-(3-dimethylaminoazetidin-1-yl)-2-methoxy-5-nitrophenyl]-4-pyrazolo[1,5-a]pyridin-3-ylpyrimidin-2-amine.*

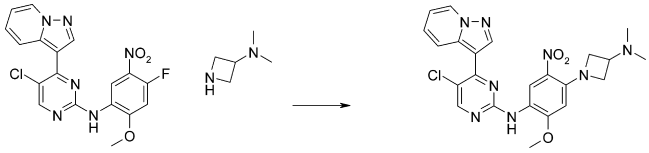

DIPEA (0.341 mL, 1.96 mmol) was added to a mixture of 5-chloro-*N*-(4-fluoro-2-methoxy-5-nitrophenyl)-4-(pyrazolo[1,5-*a*]pyridin-3-yl)-pyrimidin-2-amine (**11**, 254 mg, 0.61 mmol) and *N*,*N*-dimethylazetidin-3-amine dihydrochloride (106 mg, 0.61 mmol) in DMA (4 mL). The mixture was heated at 100 °C for 30 min. The reaction was incomplete and further *N*,*N*-dimethylazetidin-3-amine (35 mg, 0.19 mmol) was added. The mixture was stirred at 100 °C for a further 2 h and then sat at room temperature overnight.

The reaction mixture was purified directly by ion exchange chromatography, using an SCX column. The desired product was eluted from the column using 7 M NH_3/MeOH and evaporated onto silica for purification by flash silica chromatography. The crude product was purified by flash silica chromatography, with elution gradient 0−4% 7 N NH_3/MeOH in DCM. Pure fractions were evaporated to dryness to afford 5-chloro-*N*-[4-(3-dimethylaminoazetidin-1-yl)-2-methoxy-5-nitrophenyl]-4-pyrazolo[1,5-*a*]pyridin-3-ylpyrimidin-2-amine (310 mg, 102%) as an orange solid. ^{1}H NMR (400 MHz, DMSO, 30 °C) δ 2.14 (6H, s), 3.08−3.18 (1H, m), 3.76 (2H, dd), 3.89 (3H, s), 4.02−4.11 (2H, m), 6.28 (1H, s), 7.12 (1H, td), 7.3−7.39 (1H, m), 8.12 (1H, s), 8.37 (1H, br s), 8.42 (1H, s), 8.68 (1H, s), 8.83 (1H, d), 8.94 (1H, d); *m*/*z* (ES+) $(M + H)^+$ = 495.56.

N-(5-Chloro-4-pyrazolo[1,5-a]pyridin-3-ylpyrimidin-2-yl)-4-(3-dimethylaminoazetidin-1-yl)-6-methoxybenzene-1,3-diamine.

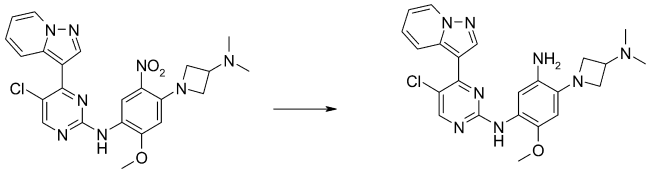

5-Chloro-*N*-[4-(3-dimethylaminoazetidin-1-yl)-2-methoxy-5-nitrophenyl]-4-pyrazolo[1,5-*a*]pyridin-3-ylpyrimidin-2-amine (265 mg, 0.54 mmol), iron (179 mg, 3.21 mmol), and ammonium chloride (20.05 mg, 0.37 mmol) were heated in ethanol (6 mL) and water (2 mL) at reflux for 1 h. The crude product was purified by ion exchange chromatography, using an SCX column. The desired product was eluted from the column using 7 M NH_3/MeOH and evaporated to dryness. Analysis showed clean product, *N*-(5-chloro-4-pyrazolo[1,5-*a*]pyridin-3-ylpyrimidin-2-yl)-4-(3-dimethylaminoazetidin-1-yl)-6-methoxybenzene-1,3-diamine (235 mg, 94%) as a yellow solid which was used directly with no further purification. ^{1}H NMR (400 MHz, DMSO, 30 °C) δ 2.13 (6H, s), 3.07 (1H, s), 3.50 (2H, t), 3.66 (3H, s), 4.00 (3H, t), 4.05 (2H, s), 6.28 (1H, s), 6.79 (1H, s), 7.10 (1H, t), 7.3−7.39 (1H, m), 8.33 (1H, s), 8.37 (1H, s), 8.80 (1H, d), 8.93 (1H, s); *m*/*z* (ES+) $(M + H)^+$ = 465.25.

N-[5-[(5-Chloro-4-pyrazolo[1,5-a]pyridin-3-ylpyrimidin-2-yl)-amino]-2-(3-dimethylaminoazetidin-1-yl)-4-methoxyphenyl]prop-2-enamide.

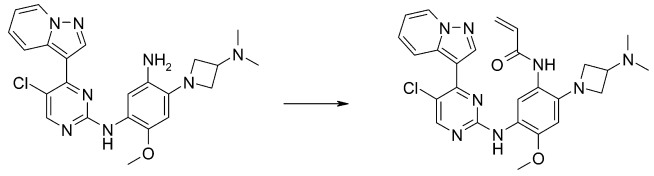

Acryloyl chloride (0.038 mL, 0.47 mmol) in DCM (1 mL) was added dropwise to a stirred solution of *N*-(5-chloro-4-pyrazolo[1,5-*a*]pyridin-3-ylpyrimidin-2-yl)-4-(3-dimethylaminoazetidin-1-yl)-6-methoxybenzene-1,3-diamine (220 mg, 0.47 mmol) and DIPEA (0.090 mL, 0.52 mmol) in DCM (5 mL), cooled in an ice/water bath. The mixture was stirred for 3 h and then washed with brine, dried (Na_2SO_4), and concentrated. The crude product was purified by flash silica chromatography, eluting with 0−5% 7 N NH_3/MeOH in DCM. Pure fractions were evaporated to dryness to afford *N*-[5-[(5-chloro-4-pyrazolo[1,5-*a*]pyridin-3-ylpyrimidin-2-yl)amino]-2-(3-dimethylaminoazetidin-1-yl)-4-methoxyphenyl]prop-2-enamide (221 mg, 90%) as a yellow solid. ^{1}H NMR (400 MHz, DMSO, 30 °C) δ 2.09 (6H, s), 3.08 (1H, p), 3.55−3.62 (2H, m), 3.76 (3H, s), 3.97 (2H, t), 5.66 (1H, dd), 6.16 (1H, dd), 6.25 (1H, s), 6.45 (1H, dd), 7.10 (1H, dd), 7.35 (1H, s), 7.39 (1H, dd), 8.25−8.4 (1H, m), 8.35 (1H, s), 8.45 (1H, s), 8.81 (1H, d), 8.92 (1H, s), 9.24 (1H, s); ^{13}C NMR (176 MHz, DMSO, 22 °C) δ 41.1, 55.5, 55.5, 56.9, 56.9, 97.2, 106.9, 113.8, 113.8, 115.8, 118.5, 120.2, 124.9, 125.1, 126.5, 128.9, 131.7, 139.1, 142.8, 144.4, 151.4, 155.2, 157.4, 159.2, 163.5. CHN analysis, $C_{26}H_{27}ClN_8O_2$ requires C = 60.17%, H = 5.24%, N = 21.59%. Found: C = 60.3%, H = 5.3%, N = 21.7%. *m*/*z* (ES+) $(M + H)^+$ = 519.56. HRMS: $(M + H)^+ = C_{26}H_{28}N_8O_2Cl$ = 519.201 82, found 519.201 90.

N-[2-(2-Dimethylaminoethylmethylamino)-4-methoxy-5-[[4-(1-methylindol-3-yl)pyrimidin-2-yl]amino]phenyl]prop-2-enamide (8). *3-(2-Chloropyrimidin-4-yl)-1H-indole.*

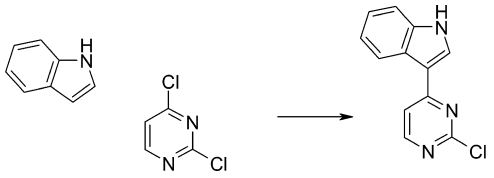

Methylmagnesium bromide (3 M in diethyl ether) (22.68 mL, 68.03 mmol) was added dropwise over a period of 10 min to a stirred solution of 1*H*-indole (7.97 g, 68.03 mmol) in 1,2-dichloroethane (250 mL) at 0 °C under nitrogen. The resulting solution was stirred for 15 min. 2,4-Dichloropyrimidine (15 g, 100.69 mmol) was added in one portion. The resulting solution was allowed to warm to ambient temperature and stirred for 16 h. The reaction was quenched by the addition of MeOH (25 mL). The mixture was evaporated to dryness, absorbed onto silica, and purified by flash silica chromatography, with elution gradient 0−20% MeOH in DCM. Pure fractions were evaporated to dryness to afford 3-(2-chloropyrimidin-4-yl)-1*H*-indole (7.17 g, 46%) as a yellow solid. ^{1}H NMR (400 MHz, DMSO, 30 °C) δ 7.2−7.28 (2H, m), 7.49−7.53 (1H, m), 7.91 (1H, d), 8.42 (1H, dd), 8.50 (1H, d), 8.53 (1H, d), 12.06 (1H, s); *m*/*z* (ES+) $(M + H)^+$ = 230.

dx.doi.org/10.1021/jm500973a | J. Med. Chem. XXXX, XXX, XXX−XXX

3-(2-Chloropyrimidin-4-yl)-1-methylindole.

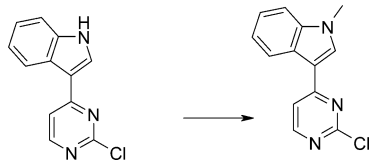

Sodium hydride (1.707 g, 42.68 mmol) was added portionwise to 3-(2-chloropyrimidin-4-yl)-1*H*-indole (8.1684 g, 35.57 mmol) in THF (250 mL) cooled to 0 °C. The resulting mixture was stirred at 0 °C for 30 min before iodomethane (2.67 mL, 42.68 mmol) was added. The mixture was stirred at 0 °C for 3 h. The reaction was quenched by the addition of saturated aqueous $NaHCO_3$ solution (25 mL). The reaction mixture was diluted with EtOAc (100 mL) and washed sequentially with saturated $NaHCO_3$ (50 mL), water (50 mL), and saturated brine (50 mL). The organic layer was evaporated to afford crude product. The crude product was purified by flash silica chromatography, with elution gradient 0−20% MeOH in DCM. Pure fractions were evaporated to dryness to afford 3-(2-chloropyrimidin-4-yl)-1-methylindole (8.35 g, 96%) as a pale yellow solid. ^{1}H NMR (400 MHz, DMSO, 30 °C) δ 3.90 (3H, s), 7.30 (2H, pd), 7.54−7.6 (1H, m), 7.82 (1H, d), 8.38−8.44 (1H, m), 8.49 (1H, s), 8.53 (1H, d); *m*/*z* (ES+) $(M + H)^+ = 244$.

Alternative Synthesis of 3-(2-Chloropyrimidin-4-yl)-1-methylindole.

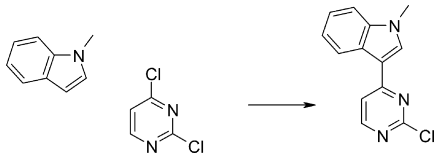

A suspension of 2,4-dichloropyrimidine (0.5 g, 3.36 mmol) and aluminum chloride (0.183 mL, 3.36 mmol) in DME (5 mL) was stirred at ambient temperature for 5 min. To this was added 1-methylindole (0.429 mL, 3.36 mmol), and the mixture was heated to 80 °C for 2 h.

The cool reaction mixture was added dropwise to vigorously stirring water (50 mL) over 5 min. Upon complete addition the mixture was stirred for 30 min, filtered and the solid washed with water (50 mL).

The crude product was purified by flash silica chromatography, eluting with DCM. Pure fractions were evaporated to dryness to afford 3-(2-chloropyrimidin-4-yl)-1-methylindole (0.515 g, 63%) as a white solid. ^{1}H NMR (400 MHz, DMSO, 30 °C) δ 3.96 (3H, s), 7.36 (2H, dqd), 7.64 (1H, dd), 7.88 (1H, d), 8.45−8.5 (1H, m), 8.56 (1H, s), 8.59 (1H, d); *m*/*z* (ES+) $(M + H)^+ = 244.54$.

N-(4-Fluoro-2-methoxy-5-nitrophenyl)-4-(1-methylindol-3-yl)-pyrimidin-2-amine.

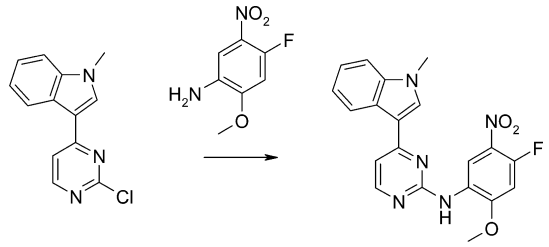

4-Methylbenzenesulfonic acid hydrate (22.73 g, 119.50 mmol) was added in one portion to 3-(2-chloropyrimidin-4-yl)-1-methylindole (24.2679 g, 99.58 mmol) and 4-fluoro-2-methoxy-5-nitroaniline[6] (18.54 g, 99.58 mmol) in 2-pentanol (500 mL). The resulting mixture was stirred at 105 °C for 2.5 h. The mixture was cooled to room temperature. The precipitate was collected by filtration, washed with 2-pentanol (50 mL), and dried under vacuum to afford *N*-(4-fluoro-2-methoxy-5-nitrophenyl)-4-(1-methylindol-3-yl)pyrimidin-2-amine as a yellow solid. The filtrate was cooled, and the precipitate was collected by filtration and washed with 2-pentanol (10 mL). The two crops were combined and triturated with MeCN to give a solid which was collected by filtration and dried under vacuum to give *N*-(4-fluoro-2-methoxy-5-nitrophenyl)-4-(1-methylindol-3-yl)pyrimidin-2-amine (37.4 g, 95%) as a yellow solid. ^{1}H NMR (400 MHz, DMSO, 30 °C) δ 3.92 (3H, s), 4.01 (3H, s), 7.13 (1H, dd), 7.27−7.36 (1H, m), 7.4−7.51 (2H, m), 7.59 (1H, d), 8.26 (1H, t), 8.35 (1H, d), 8.61 (1H, s), 8.85 (1H, d), 9.46 (1H, s); *m*/*z* (ES−) $M^- = 392$.

N′-(2-Dimethylaminoethyl)-2-methoxy-N′-methyl-N-[4-(1-methylindol-3-yl)pyrimidin-2-yl]-5-nitrobenzene-1,4-diamine.

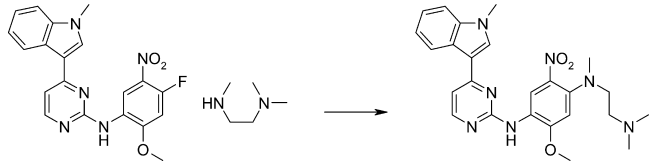

*N*1,*N*1,*N*2-Trimethylethane-1,2-diamine (80 mg, 0.79 mmol) was added to a suspension of *N*-(4-fluoro-2-methoxy-5-nitrophenyl)-4-(1-methylindol-3-yl)pyrimidin-2-amine (350 mg, 0.79 mmol) and DIPEA (0.342 mL, 1.97 mmol) in 2,2,2-trifluoroethanol (5 mL). The mixture was heated in a microwave at 140 °C for 60 min.

The cooled reaction mixture was purified by ion exchange chromatography, using an SCX column. The desired product was eluted from the column using 7 M NH_3/MeOH and evaporated onto silica for silica chromatography. The crude product was purified by flash silica chromatography, with elution gradient 0−4% 7 N NH_3/MeOH in DCM. Pure fractions were evaporated to dryness to afford *N′*-(2-dimethylaminoethyl)-2-methoxy-*N′*-methyl-*N*-[4-(1-methylindol-3-yl)pyrimidin-2-yl]-5-nitrobenzene-1,4-diamine (230 mg, 62%) as an orange solid. ^{1}H NMR (400 MHz, DMSO, 22 °C) δ 2.16 (6H, s), 2.45−2.49 (2H, t), 2.86 (3H, s), 3.26 (2H, t), 3.87 (3H, s), 3.95 (3H, s), 6.85 (1H, s), 7.11 (1H, t), 7.21 (1H, d), 7.25 (1H, t), 7.52 (1H, d), 8.10 (1H, s), 8.31 (1H, d), 8.33 (1H, s), 8.36 (1H, d), 8.62 (1H, s); *m*/*z* (ES+) $(M + H)^+ = 476.40$.

N1-(2-Dimethylaminoethyl)-5-methoxy-N1-methyl-N4-[4-(1-methylindol-3-yl)pyrimidin-2-yl]benzene-1,2,4-triamine.

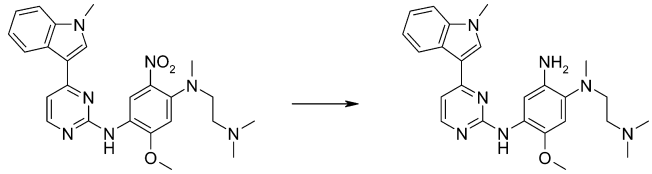

N′-(2-Dimethylaminoethyl)-2-methoxy-*N′*-methyl-*N*-[4-(1-methylindol-3-yl)pyrimidin-2-yl]-5-nitrobenzene-1,4-diamine (220 mg, 0.46 mmol), iron (155 mg, 2.78 mmol), and ammonium chloride (17.32 mg, 0.32 mmol) were heated in ethanol (12 mL) and water (4 mL) at reflux for 2 h. The crude product was purified by ion exchange chromatography, using an SCX column. The desired product was eluted from the column using 7 M NH_3/MeOH and evaporated onto silica for chromatographic purification.

The crude product was purified by flash silica chromatography, with elution gradient 0−5% 7N NH_3/MeOH in DCM. Pure fractions were evaporated to dryness to afford *N*1-(2-dimethylaminoethyl)-5-methoxy-*N*1-methyl-*N*4-[4-(1-methylindol-3-yl)pyrimidin-2-yl]benzene-1,2,4-triamine (175 mg, 85%) as a beige foam. ^{1}H NMR (400 MHz, DMSO, 22 °C) δ 2.17 (6H, s), 2.36 (2H, t), 2.63 (3H, s), 2.88 (2H, t), 3.74 (3H, s), 3.88 (3H, s), 4.58 (2H, br s), 6.76 (1H, s), 7.12−7.19 (2H, m), 7.21−7.27 (1H, m), 7.48 (1H, s), 7.51 (1H, d), 7.78 (1H, s), 8.27 (1H, d), 8.30 (1H, s), 8.42 (1H, d); *m*/*z* (ES+) $(M + H)^+ = 446.32$.

N-[2-(2-Dimethylaminoethylmethylamino)-4-methoxy-5-[[4-(1-methylindol-3-yl)pyrimidin-2-yl]amino]phenyl]prop-2-enamide.

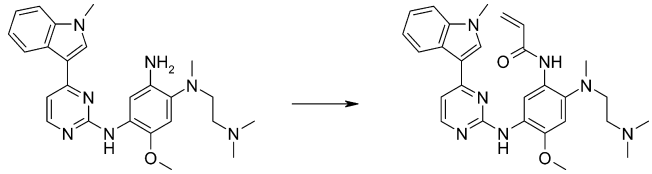

Acryloyl chloride (34.5 mg, 0.38 mmol) in DCM (1 mL) was added dropwise to a stirred solution of *N*1-(2-dimethylaminoethyl)-5-methoxy-*N*1-methyl-*N*4-[4-(1-methylindol-3-yl)pyrimidin-2-yl]-benzene-1,2,4-triamine (170 mg, 0.38 mmol) and DIPEA (0.073 mL, 0.42 mmol) in DCM (5 mL), cooled in an ice/water bath. The mixture was stirred for 90 min and then diluted with DCM (25 mL) and washed with saturated aqueous $NaHCO_3$ solution (50 mL). The organics were

dx.doi.org/10.1021/jm500973a | *J. Med. Chem.* XXXX, XXX, XXX−XXX

removed, and the aqueous portion was further extracted with DCM (2 × 25 mL). The combined organics were dried over $MgSO_4$, filtered, and concentrated onto silica for purification. The crude product was purified by flash silica chromatography, with elution gradient 0−4% 7 N NH_3/MeOH in DCM. Pure fractions were evaporated to dryness and triturated with ether to afford *N*-[2-(2-dimethylaminoethylmethylamino)-4-methoxy-5-[[4-(1-methylindol-3-yl)pyrimidin-2-yl]amino]phenyl]prop-2-enamide (75 mg, 39%) as a cream solid. ^{1}H NMR (400 MHz, DMSO, 22 °C) δ 2.21 (6H, s), 2.29 (2H, t), 2.72 (3H, s), 2.89 (2H, t), 3.86 (3H, s), 3.92 (3H, s), 5.77 (1H, dd), 6.27 (1H, dd), 6.43 (1H, dd), 7.04 (1H, s), 7.15 (1H, t), 7.2−7.27 (2H, m), 7.53 (1H, d), 7.91 (1H, s), 8.24 (1H, d), 8.33 (1H, d), 8.68 (1H, s), 9.14 (1H, s), 10.22 (1H, s); ^{13}C NMR (176 MHz, DMSO, 22 °C) δ 32.8, 42.6, 45.1, 55.7, 56.0, 56.8, 105.3, 107.1, 110.4, 112.4, 113.3, 120.8, 121.2, 121.9, 125.3, 125.5, 125.9, 127.7, 132.4, 133.8, 137.3, 137.7, 145.8, 157.6, 158.9, 159.8, 161.5, 162.3. CHN analysis, $C_{28}H_{33}N_7O_2{\cdot}H_2O$ requires C = 64.97%, H = 6.82%, N = 18.94%. Found: C = 64.6%, H = 6.7%, N = 18.8%. *m/z* (ES+) $(M + H)^+$ = 500.42. HRMS: $(M + H)^+ = C_{28}H_{34}N_7O_2$ = 500.276 84, found 500.276 86.

N-[2-(2-Dimethylaminoethylmethylamino)-4-methoxy-5-[[4-(1-methylindol-3-yl)pyrimidin-2-yl]amino]phenyl]prop-2-enamide Mesylate Salt.

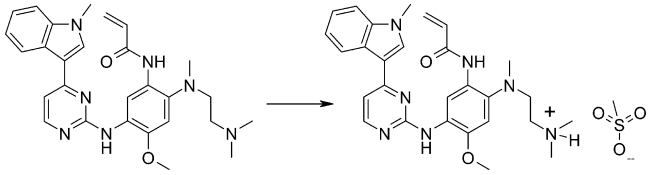

To a stirred solution of *N*-[2-(2-dimethylaminoethylmethylamino)-4-methoxy-5-[[4-(1-methylindol-3-yl)pyrimidin-2-yl]amino]phenyl]-prop-2-enamide (5g, 9.11 mmol) in acetone (45.5 mL) and water (4.55 mL) at 50 °C was added methanesulfonic acid (0.893g, 9.11 mmol) as a solution in acetone (4.55 mL). The resulting mixture was stirred for 1.5 h. The resulting solid was collected by filtration and dried at 80 °C under vacuum to give the title salt (4.9 g, 94%) as a solid (mp(DSC) = 246−259 °C). ^{1}H NMR (400 MHz, acetone-d_6, 22 °C) δ 2.72 (3H, s), 2.96 (3H, s), 3.01 (6H, s), 3.58 (3H, t), 3.87−3.90 (7H, m), 5.76 (1H, dd), 6.38−6.53 (2H, m), 7.12 (1H, t), 7.20 (1H, t), 7.29 (1H, s), 7.40 (2H, t), 8.07−8.16 (3H, m), 8.56 (1H, s), 9.30 (1H, s), 9.60 (1H, s), 9.66 (1H, s); ^{13}C NMR (101 MHz, acetone-d_6, 22 °C) δ 34.3, 39.9, 44, 45.5, 50.1, 55.2, 57, 105.9, 107.7, 112, 113.4, 123.4, 123.9, 124.4, 124.9, 125.1, 125.2, 126.9, 129.4, 131.5, 139.9, 140.2, 142.3, 144, 152.8, 153.7, 167.1, 169.3. CHN analysis, $C_{29}H_{37}O_5N_7S$ (0.1% w/w H_2O) requires C = 58.41%, H = 6.27%, N = 16.44%, S = 5.38%. Found: C = 58.6%, H = 6.3%, N = 16.5%, S = 5.2%. *m/z* (ES+) $(M + H)^+$ = 500.26. HRMS: $(M + H)^+ = C_{28}H_{34}N_7O_2$ = 500.27684, found 500.2759.

Cellular Assays. Cellular phosphorylation and proliferation assays were performed as reported previously by ourselves.[6]

In Vivo Antitumor Efficacy Studies. All in vivo efficacy studies were performed as reported previously by ourselves.[6]

Rat in Vivo Toxicology Studies. Studies were carried out in accordance with U.K. Home Office legislation (Animals [Scientific Procedures] Act 1986) and AstraZeneca's institutional policies. The animals used were 10-week-old male RccHan:WIST rats obtained from Harlan, U.K. Animals (n = 3/compound) received a single oral dose of compound as a suspension in 0.5% w/v HPMC/0.1% w/v Tween in deionized water at a concentration of 20 mg/mL. Blood glucose levels were measured using an Accuchek Active meter (ACCU-CHEK Active; Roche, Basel, Switzerland). Serum insulin concentrations were determined using a commercial rat ELISA kit (Mercodia, Upsala, Sweden). Water and food were available ad libitum.

■ ASSOCIATED CONTENT

Supporting Information

Preparation and characterization for additional final compounds, cell assay statistical analyses, pharmacodynamic assay procedure, kinase selectivty data, binding mode computational modeling, and enzyme/cell correlations. This material is available free of charge via the Internet at http://pubs.acs.org.

■ AUTHOR INFORMATION

Corresponding Author

*E-mail: ray.finlay@astrazeneca.com. Phone: +44(0)1625510379.

Notes

The authors declare no competing financial interest.

■ ACKNOWLEDGMENTS

The authors thank Didier Danillion, Gareth Hughes, Cath Eberlein, and Scott Martin for expert technical assistance. We are also grateful to Anne Galer and Paula Daunt for project team leadership. We also acknowldege Susan Galbraith for her support of the AZD9291 program. Jamie Scott, Jason Kettle, and Kevin Foote are also gratefully acknowledged for their helpful comments during the preparation of this manuscript.

■ ABBREVIATIONS USED

EGFR, epidermal growth factor receptor; NSCLC, non-small-cell lung cancer; TKI, tyrosine kinase inhibitor; GSH, glutathione; PK, pharmacokinetics; WT, wild-type; AM, activating mutant; DM, double mutant; LLE, ligand lipophilicity efficiency; LCMS, liquid chromatography−mass spectrometry; SAR, structure−activity relationship; HPLC, high-performance liquid chromatography; DCM, dichloromethane; DMA, *N*,*N*-dimethylacetamide; DMF, *N*,*N*-dimethylformamide; DIPEA, *N*,*N*-diisopropylethylamine; DMSO, dimethyl sulfoxide; TBAF, tetra-*N*-butylammonium fluoride; TFA, trifluoroacetic acid; THF, tetrahydrofuran

■ REFERENCES

(1) Ohashi, K.; Maruvka, Y. E.; Michor, F.; Pao, W. Epidermal growth factor receptor tyrosine kinase inhibitor-resistant disease. *J. Clin. Oncol* **2013**, *31*, 1070−1080.

(2) Pao, W.; Chmielecki, J. Rational, biologically based treatment of EGFR-mutant non-small-cell lung cancer. *Nat. Rev. Cancer* **2010**, *10*, 760−774.

(3) Maemondo, M.; Inoue, A.; Kobayashi, K.; Sugawara, S.; Oizumi, S.; Isobe, H.; Gemma, A.; Harada, M.; Yoshizawa, H.; Kinoshita, I.; Fujita, Y.; Okinaga, S.; Hirano, H.; Yoshimori, K.; Harada, T.; Ogura, T.; Ando, M.; Miyazawa, H.; Tanaka, T.; Saijo, Y.; Hagiwara, K.; Morita, S.; Nukiwa, T. Gefitinib or chemotherapy for non-small-cell lung cancer with mutated EGFR. *N. Engl. J. Med.* **2010**, *362*, 2380−2388.

(4) Kobayashi, S.; Boggon, T. J.; Dayaram, T.; Jaenne, P. A.; Kocher, O.; Meyerson, M.; Johnson, B. E.; Eck, M. J.; Tenen, D. G.; Halmos, B. EGFR mutation and resistance of non-small-cell lung cancer to gefitinib. *N. Engl. J. Med.* **2005**, *352*, 786−792.

(5) Ou, S.-H. I. Second-generation irreversible epidermal growth factor receptor (EGFR) tyrosine kinase inhibitors (TKIs): A better mousetrap? A review of the clinical evidence. *Crit. Rev. Oncol. Hematol.* **2012**, *83*, 407−421.

(6) Ward, R. A.; Anderton, M. J.; Ashton, S.; Bethel, P. A.; Box, M.; Butterworth, S.; Colclough, N.; Chorley, C. G.; Chuaqui, C.; Cross, D. A.; Dakin, L. A.; Debreczeni, J. E.; Eberlein, C.; Finlay, M. R. V.; Hill, G. B.; Grist, M.; Klinowska, T. C.; Lane, C.; Martin, S.; Orme, J. P.; Smith, P.; Wang, F.; Waring, M. J. Structure- and reactivity-based development of covalent inhibitors of the activating and gatekeeper mutant forms of the epidermal growth factor receptor (EGFR). *J. Med. Chem.* **2013**, *56*, 7025−7048.

(7) Zhou, W.; Ercan, D.; Chen, L.; Yun, C.-H.; Li, D.; Capelletti, M.; Cortot, A. B.; Chirieac, L.; Iacob, R. E.; Padera, R.; Engen, J. R.; Wong, K.-K.; Eck, M. J.; Gray, N. S.; Janne, P. A. Novel mutant-selective EGFR kinase inhibitors against EGFR T790M. *Nature* **2009**, *462*, 1070−1074.

(8) Walter, A. O.; Sjin, R. T. T.; Haringsma, H. J.; Ohashi, K.; Sun, J.; Lee, K.; Dubrovskiy, A.; Labenski, M.; Zhu, Z.; Wang, Z.; Sheets, M.; St Martin, T.; Karp, R.; van Kalken, D.; Chaturvedi, P.; Niu, D.; Nacht, M.; Petter, R. C.; Westlin, W.; Lin, K.; Jaw-Tsai, S.; Raponi, M.;

Van Dyke, T.; Etter, J.; Weaver, Z.; Pao, W.; Singh, J.; Simmons, A. D.; Harding, T. C.; Allen, A. Discovery of a mutant-selective covalent inhibitor of EGFR that overcomes T790M-mediated resistance in NSCLC. *Cancer Discovery* **2013**, *3*, 1404−1415.
(9) (a) International Centre for Kinase Profiling. http://www.kinase-screen.mrc.ac.uk/ (accessed August 12, 2014). (b) Compounds were screened in the Millipore kinase panel. Full data are described in ref 20.
(10) Yee, D. Insulin-like growth factor receptor inhibitors: baby or the bathwater? *J. Natl. Cancer Inst.* **2012**, *104*, 975−981.
(11) Clarke, E. D.; Greenhow, D. T.; Adams, D. Metabolism-related assays and their application to agrochemical research: reactivity of pesticides with glutathione and glutathione transferases. *Pestic. Sci.* **1998**, *54*, 385−393.
(12) MacFaul, P. A.; Morley, A. D.; Crawford, J. J. A simple in vitro assay for assessing the reactivity of nitrile containing compounds. *Bioorg. Med. Chem. Lett.* **2009**, *19*, 1136−1138.
(13) Schwobel, J. A. H.; Madden, J. C.; Cronin, M. T. D. Examination of Michael addition reactivity towards glutathione by transition-state calculations. *SAR QSAR Environ. Res.* **2010**, *21*, 693−710.
(14) Mah, R.; Thomas, J. R.; Shafer, C. M. Drug discovery considerations in the development of covalent inhibitors. *Bioorg. Med. Chem. Lett.* **2014**, *24*, 33−39.
(15) Marks, L.; Borland, S.; Philip, K.; Ewart, L.; Lainée, P.; Skinner, M.; Kirk, S.; Valentin, J. P. The role of the anaesthetised guinea-pig in the preclinical cardiac safety evaluation of drug candidate compounds. *Toxicol. Appl. Pharmacol.* **2012**, *263*, 171−83.
(16) Eurofins. Discovery Series. KinaseProfiler Services. http://www.eurofins.com/pharma-services/pharma-discovery-services/eurofins-discovery-services/kinases-phosphatases/kinaseprofiler-services.aspx (accessed August 12, 2014).
(17) Tang, W.; Stearns, R. A.; Chen, Q.; Bleasby, K.; Teffera, Y.; Colletti, A.; Hafey, M.; Evers, R.; Dean, D. C.; Magriotis, P. A. Importance of mechanistic drug metabolism studies in support of drug discovery: a case study with N-sulfonylated dipeptide VLA-4 antagonists in rats. *Xenobiotica* **2008**, *38*, 223−237.
(18) El-Kattan, A. F.; Poe, J.; Buchholz, L.; Thomas, H. V.; Brodfuehrer, J.; Clark, A. The use of 1-aminobenzotriazole in differentiating the role of CYP-mediated first pass metabolism and absorption in limiting drug oral bioavailability: a case study. *Drug Metab. Lett.* **2008**, *2*, 120−124.
(19) Manley, P. W.; Blasco, F.; Mestan, J.; Aicholz, R. The kinetic deuterium isotope effect as applied to metabolic deactivation of imatinib to the des-methyl metabolite CGP74588. *Bioorg. Med. Chem.* **2013**, *21*, 3231−3239.
(20) Sjogren, E.; Westergren, J.; Grant, I.; Hanish, G.; Lindfors, L.; Lennernas, H.; Abrahamsson, B.; Tannergren, C. In silico predictions of gastrointestinal drug absorption in pharmaceutical product development: application of the mechanistic absorption model GI-Sim. *Eur. J. Pharm. Sci.* **2013**, *49*, 679−698.
(21) (a) Ballard, P.; Ashton, S.; Cross, D.; Dimelow, R.; Yates, J. Integrating the pre-clinical pharmacokinetic, pharmacodynamic and efficacy data for AZD9291, an oral, irreversible inhibitor of EGFR activating (EGFRm+) and resistant (EGFRm+/T790M) mutations and an active metabolite to predict the human pharmacokinetics and potential efficacious dose in patients. *Mol. Cancer Ther* **2013**, *12* (11 Suppl.), B212. (b) Cross, D. A. E.; Ashton, S.; Ghiorghiu, S.; Eberlein, C.; Nebhan, C.; Spitzler, P.; Orme, J.; Finlay, M. R. V.; Ward, R. A.; Mellor, M.; Hughes, G.; Rahi, A.; Jacobs, V.; Red Brewer, M.; Ichihara, E.; Sun, J.; Jin, H.; Ballard, P.; Al-Kadhimi, K.; Rowlinson, R.; Klinowska, T.; Richmond, G.; Cantarini, M.; Kim, D.-W.; Ranson, M.; Pao, W. AZD9291, an irreversible EGFR TKI, overcomes T790M-mediated resistance to EGFR inhibitors in lung cancer. *Cancer Discovery* **2014**, *4*, 1046−1061.
(22) Ranson, M.; Pao, W.; Planchard, D.; Ohe, Y.; Kim, S.-W.; Kim, D. W.; Felip, E.; Ghiorghiu, S.; Cantarini, M.; Janne, P. Preliminary results from a phase I study with AZD9291: an irreversible inhibitor of epidermal growth factor receptor (EGFR) activating and resistance mutations in non-small-cell lung cancer (NSCLC). *Eur. J. Cancer* **2013**, *49* (Suppl. 3), S15 (Abstract LBA33).
(23) Eisenhauer, E. A.; Therasse, P.; Bogaerts, J.; Schwartz, L. H.; Sargent, D.; Ford, R.; Dancey, J.; Arbuck, S.; Gwyther, S.; Mooney, M.; Rubinstein, L.; Shankar, L.; Dodd, L.; Kaplan, R.; Lacombe, D.; Verweij, J. New response evaluation criteria in solid tumours: Revised RECIST guideline (version 1.1). *Eur. J. Cancer* **2009**, *45*, 228−247.
(24) Common Terminology Criteria for Adverse Events (CTCAE). http://evs.nci.nih.gov/ftp1/CTCAE/CTCAE_4.03_2010-06-14_QuickReference_5x7.pdf (accessed August 12, 2014).
(25) Janne, P. A.; Ramaligam, S. S.; Yang, J. C. H.; Ahn, M.-J.; Kim, D.-W.; Kim, S.-W.; Planchard, D.; Ohe, Y.; Felip, E.; Watkins, C.; Cantarini, M.; Ghiorghiu, S.; Ranson, M. Clinical activity of the mutant-selective EGFR inhibitor AZD9291 in patients (pts) with EGFR inhibitor−resistant non-small-cell lung cancer (NSCLC). *J. Clin Oncol* **2014**, *32* (Suppl. 5), 8009.